Nanoscale

Accepted Manuscript

This article can be cited before page numbers have been issued, to do this please use: A. Shibata, M. Nuno, T. Ishikawa, H. Kasai and K. Oka, *Nanoscale*, 2026, DOI: 10.1039/D5NR05521K.

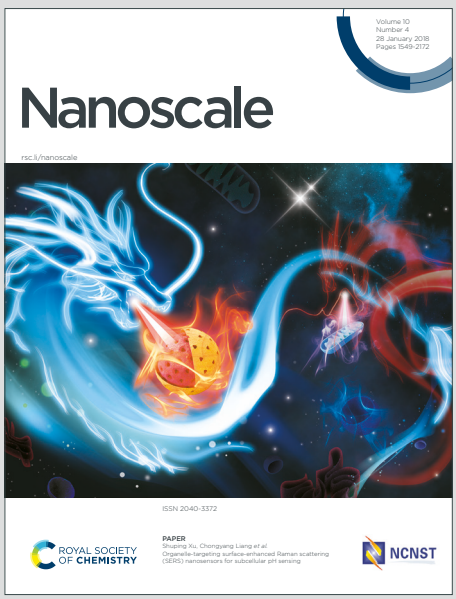

ROYAL SOCIETY OF CHEMISTRY

rsc.li/nanoscale

View Article Online
DOI: 10.1039/D5NR05521K

REVIEW

Mechanisms and Potential Applications of Technologies for Detecting Specific Polyfluoroalkyl Substances *via* Nano-level Interactions

Received 00th January 20xx,
Accepted 00th January 20xx

DOI: 10.1039/x0xx00000x

Aki Shibata,*[a] Mitsuaki Nuno,[b] Tomoka Ishikawa,[a] Hitoshi Kasai,[a] Kouki Oka*[a,c,d]

Per- and polyfluoroalkyl substances, possessing chemically and thermally stable C-F bonds, have been widely used in various products owing to their flame retardancy, chemical resistance, and water- and oil-repellent characteristics. Among these, some perfluoroalkyl substances ('specific **PFAS**') are beginning to raise concerns regarding their potential toxicity to living organisms and bioaccumulation. Recently, specific **PFAS** originating from fire-extinguishing foam, wastewater from semiconductor manufacturing plants, and fluororesin-coated waste have been detected in aqueous environments worldwide. These species mainly present at low concentrations (parts-per-trillion (ppt) level) and have prompted stringent regulations, such as drinking water standards. Liquid chromatography–tandem mass spectrometry remains the gold standard for detecting specific **PFAS** at the ppt level. However, its implementation necessitates skilled handling and long analysis durations. To address these problems, based on interactions with specific **PFAS** at the nano-level, there has been active development of materials aimed at detecting specific **PFAS** with high sensitivity, simply, and in a short time. Several materials capable of detecting specific **PFAS** at parts-per-billion (ppb) to parts-per-million (ppm) levels are already undergoing verification research with a view to practical application. Nevertheless, the detection technologies of specific **PFAS** at the ppt level in actual aqueous environments remains challenging owing to limited selectivity against contaminants and difficulty in widespread on-site detection. This review provides a comprehensive overview of detection material and technologies for specific **PFAS**. Moreover, we comprehensively discuss the detection mechanisms and sensing performance of specific **PFAS** detection materials, as well as issues facing practical application, and present future prospects for materials and material development aimed at the simple, rapid, and highly sensitive detection of specific **PFAS**.

1. Introduction

PFAS are a general term for fluorinated substances that contain at least oneflully fluorinated methyl or methylene carbon atom.[1-3] Among these compounds, those with a hydrophobic methylene backbone and hydrophilic terminal functional groups (e.g., -COOH and -SO_3H) exhibit surfactant properties (**Figure 1**).[4-6] **PFAS** have been extensively used in a wide range of industrial and consumer products, including fire-extinguishing foams, semiconductor manufacturing, water-repellent coatings, and food packaging, due to their flame retardancy, chemical resistance, and water and oil repellency, which stem from their inertness, high durability, and low surface energy of the C-F bond.[7-17] In contrast, certain **PFAS** ('specific **PFAS**') emitted, leaked or leached from manufacturing facilities and waste products have been increasingly detected in public water bodies and groundwater through wastewater discharge and precipitation.[18-22] The C-F bond in **PFAS** exhibits the highest bond dissociation energy (approximately 485 kJ/mol) among covalent single bonds in organic compounds, which renders it extremely chemically and thermally stable.[23-26]

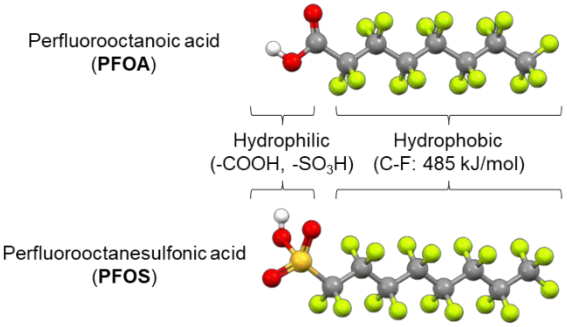

Figure 1 Chemical structures of representative 'specific **PFAS**', such as **PFOA** and **PFOS** (hydrophilic moieties: -COOH, -SO_3H; hydrophobic moiety: carbon chain with C-F bond (485 kJ/mol)).

[a] *Institute of Multidisciplinary Research for Advanced Materials, Tohoku University, 2-1-1 Katahira, Aoba-ku, Sendai, Miyagi 980-8577, Japan*
[b] *Kubota Corporation, 1-1-1, Hama, Amagasaki, Hyogo 661-8567, Japan*
[c] *Carbon Recycling Energy Research Center, Ibaraki University, 4-12-1, Nakanarusawacho, Hitachi, Ibaraki 316-0033, Japan*
[d] *Deuterium Science Research Unit, Center for the Promotion of Interdisciplinary Education and Research, Kyoto University, Yoshida, Sakyo-ku, Kyoto 606-8501, Japan.*

** oka@tohoku.ac.jp (Kouki Oka)*
** aki.shibata.d5@tohoku.ac.jp (Aki Shibata)*

Supplementary Information available: [details of any supplementary information available should be included here]. See DOI: 10.1039/x0xx00000x

View Article Online
DOI: 10.1039/D5NR05521K

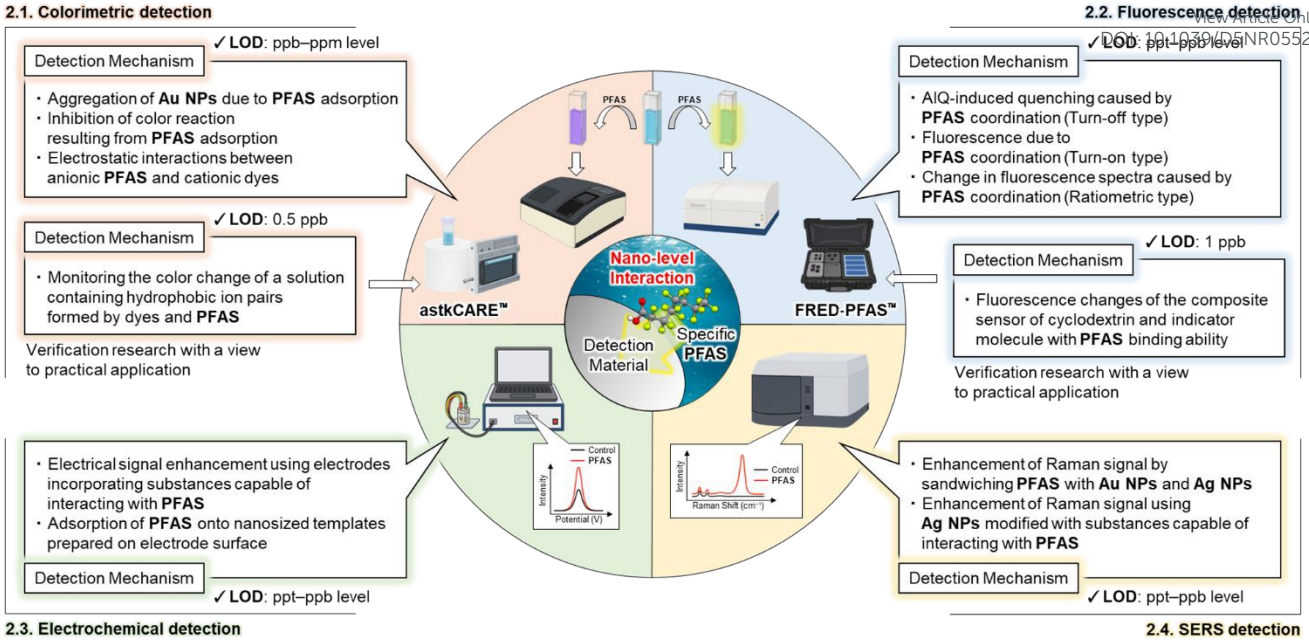

Figure 2 Overview of specific **PFAS** detection technologies discussed in Sections 2.1 to 2.4 (**colorimetric**, **fluorescence**, **electrochemical**, **and SERS detection**) and their detection mechanisms based on nanolevel interactions with specific **PFAS**. (Abbreviations: **SERS**: surface-enhanced Raman scattering; **LOD**: limit of detection; **Au NPs**: gold nanoparticles; **Ag NPs**: silver nanoparticles; AIQ: aggregation-induced quenching)

Consequently, **PFAS** are highly resistant to decomposition in aqueous environments and persist as 'forever chemicals'.[27, 28]

In recent years, living organisms have been exposed to **PFAS** through drinking and domestic water.[29-33] Specific **PFAS**[34, 35] such as perfluorooctanoic acid (**PFOA**) and perfluorooctanesulfonic acid (**PFOS**), have raised concerns about their potential for toxicity to living organisms, including carcinogenicity,[36, 37] immunosuppression,[38, 39] endocrine disruption,[40, 41] and bioaccumulation.[42-47] In particular, these specific **PFAS** have been reported to be detected at high concentrations (several ppm levels) in water bodies near certain areas such as fire training grounds and semiconductor manufacturing plants.[48, 49] Consequently, many countries worldwide have begun regulating the concentrations of specific **PFAS** in aqueous environments, while strengthening their monitoring to promote environmental and health management. The World Health Organization has proposed a guideline limit of 100 ppt for the total concentration of **PFAS** in drinking water and is aiming for a strict management system.[50] Several countries have established more stringent drinking-water standards. For example, the U.S. Environmental Protection Agency (EPA) sets a limit of 4 ppt for **PFOA** and **PFOS** respectively,[51] while Denmark has established a limit of 2 ppt for the combined concentration of **PFOA**, **PFOS**, perfluorohexanesulfonic acid, and perfluorononanoic acid (**PFNA**).[52]

Specific **PFAS** in aqueous environments are typically present at ppt levels,[53-57] necessitating ultrasensitive detection technologies. Liquid chromatography-tandem mass spectrometry (LC-MS/MS), the current gold standard, can detect specific **PFAS** at the ppt level.[58] However, the analysis is cost- and time-intensive (USD 200–300 per sample; half a day – more than a day to measure **PFAS**-containing samples (it is estimated that the process from sample collection to receiving the measurement results from the external contractor takes 2–6 weeks.)[59]) and requires expensive equipment (USD 1,000,000–2,000,000) and skilled technicians.[60, 61] As regular monitoring systems for specific **PFAS** begin to be established globally, LC-MS/MS measurements of all water bodies and industrial sites suspected of contamination are not feasible.[62]

Based on the above, alternative detection technologies are being investigated to enable prompt, facile, and low-cost detection of specific **PFAS** in aqueous environments. Many of these technologies are based on nano-level interactions between the detection materials and specific **PFAS** (**Figure 2**). This review provides a comprehensive overview of specific **PFAS** detection research reported in recent years, focusing on nano-level interactions-based detection mechanisms and sensing performance. This review systematically summarizes the detection mechanism of each detection research, along with its limit of detection (**LOD**), detection time, measurement solvent, interfering species, and detection selectivity. In addition, based on a systematic comparison of specific **PFAS** detection research, it discusses challenges for applying the research to actual aqueous environments and presents requirements for future development prospects.

2. Nano-level interactions-based detection of specific PFAS

Recent major research enabling rapid, low-cost, and simple detection of specific **PFAS** were classified based on differences in detection mechanisms. **2.1. Colorimetric detection** involves observing changes in absorbance due to the interaction of specific **PFAS** with the surface of a detection material. **2.2. Fluorescence**

View Article Online
DOI: 10.1039/D5NR05521K

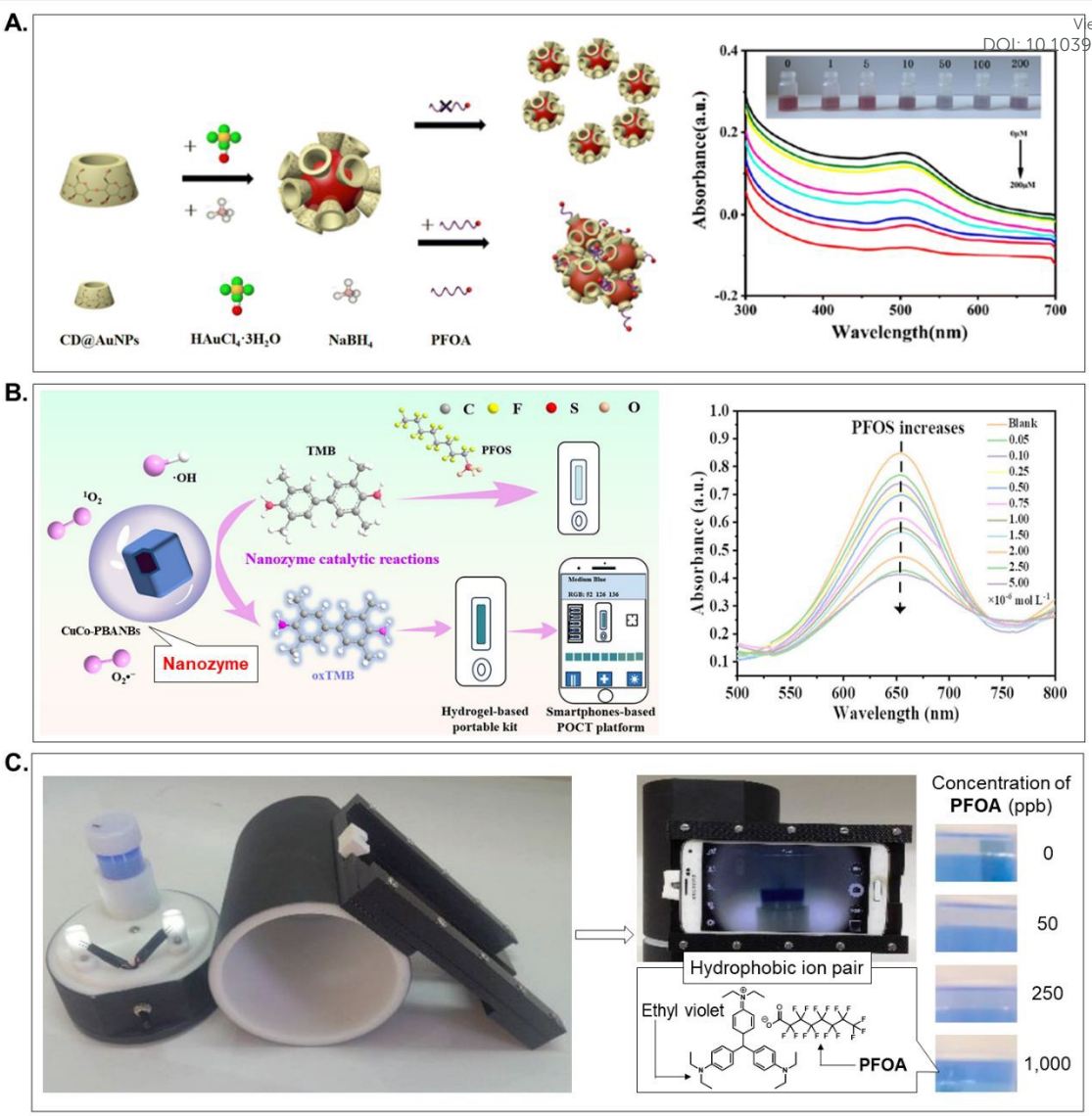

Figure 3 Schematic of colorimetric detection mechanism of specific **PFAS**: (A) aggregation induced by specific **PFAS** adsorption on **Au NP** surfaces; (B) inhibition of colouration resulting from specific **PFAS** adsorption onto the surface of nanozymes catalysing ROS generation; (C) monitoring the colour change of a solution containing hydrophobic ion pairs formed by dyes and specific **PFAS** using **astkCARE™**) Reproduced with permissions from ref. 63, Copyright 2025 Royal Society of Chemistry; ref. 65, Copyright 2024 American Chemical Society; and ref. 80 Copyright 2018 Elsevier.

detection involves detecting changes in the excitation state of the material or the energy transfer process associated with the interaction between the specific **PFAS** and the detection material, resulting in a fluorescent signal. **2.3. Electrochemical detection** involves converting the interaction between specific **PFAS** and nanostructures on the electrode surface into an electrical signal. **2.4. Surface-enhanced Raman scattering (SERS) detection** utilizes the interaction between specific **PFAS** and nanometal surfaces to detect vibrational spectra with high sensitivity. This review focuses on major research that utilize the detection mechanism based on nano-level interactions with these specific **PFAS**, and outlines the detection process for specific **PFAS**, the detection ability for **PFAS** (**PFAS** as a single substance such as **PFOA** and **PFOS**), the reactivity of detection materials to contaminants such as ions and surfactants, and challenges for practical application.

2.1. Colorimetric detection

Colorimetric detection based on nano-level interactions with specific **PFAS** can be divided into three categories, based on the [1] aggregation state of the detection material, [2] catalytic reaction of the detection material (nanozyme), and [3] absorbance of dyes that form hydrophobic ion pairs and F-F interactions. These methods are being explored as promising strategies for the rapid and simple on-site detection of specific **PFAS**.

[1] In aggregation-based detection, the detection material aggregates through interaction with specific **PFAS**, allowing detection as changes in the absorption spectrum or visible colour (**Figure 3A**)[63]. This method commonly involves gold nanoparticles (**Au NPs**), which exhibit colour transitions between dispersed and aggregated states owing to plasmon resonance. The surface of **Au NPs** is typically modified with

functional groups that can enhance reactivity with specific **PFAS**. For example, Ma *et al.* prepared cyclodextrin (**CD**)-modified **Au NPs** (**CD@Au NPs**) and achieved a **LOD** of 70.4 ppb for **PFOA** within 1 h (without solid-phase extraction (**SPE**)), leveraging host–guest interactions in a water/*N*,*N*-dimethylformamide (DMF) mixed solution.[63] Jung *et al.* synthesized **citrate-coated Au NPs**, which were surface-modified with perfluoroalkyl chains (carbon chain length of 6 or more).[64] In the **citrate-coated Au NPs**, after mixing the **NPs** with multiple types of **PFAS** (perfluorohexanoic acid (**PFHxA**), **PFNA**, perfluorodecanoic acid (**PFDA**), and perfluorooctyl phosphonic acid (**PFOPA**) each as a single substance) in water, the **citrate-coated Au NPs** could be detected from the change in absorption spectrum over time associated with the aggregation of NPs with different amounts of PFAS attached due to differences in F-F interactions with the perfluoroalkyl chain, exhibiting the **LOD** of 42.7–2,005 ppb (without **SPE**). These **NPs** showed high reactivity to long-chain **PFAS** (such as **PFDA** and **PFNA**) that easily undergo F-F interactions with perfluoroalkyl chains, and the absorption spectrum immediately changed with the addition of a small amount of **PFAS**. Unfortunately, the selectivity of these **NPs** for detecting specific **PFAS** was low, and the increase in hydrophobic interactions due to the adsorption of dissolved organic matter other than specific **PFAS** and the decrease in electrostatic interactions due to changes in pH may also cause **NPs** to aggregate, potentially affecting the time-dependent changes in absorption spectrum after addition of **PFAS**. As these detection mechanisms rely on aggregation of **NPs**, controlling dispersion stability–such as through surface modification of **NPs** using surfactants structurally dissimilar to **PFAS**, ensuring aggregation occurs only upon interaction with **PFAS**–may potentially suppress reactivity to contaminants. Nonetheless, due to the evaluation of changes in absorbance and absorption spectrum at the same wavelength, this method is expected to be difficult to detect and identify between different types and concentrations of **PFAS** in the presence of multiple **PFAS**. Consequently, aggregation-based methods using **Au NPs** typically achieve **LOD** only in the tens-of-ppb range.[63, 64]

[2] Catalytic-reaction-based detection uses nanozymes, composed of metal oxides or carbon materials, that catalyse the production of reactive oxygen species (ROS) (**Figure 3B**).[65] Detection is accomplished by comparing the colorimetric response of 3,3',5,5'-tetramethylbenzidine (TMB) in the presence and absence of specific **PFAS**. The nanozyme detects specific **PFAS** through the following process: (1) The colourless TMB is oxidized by ROS generated on the nanozyme surface and turns blue. (2) When specific **PFAS** adsorb onto the nanozyme surface, ROS generation is inhibited, and no colouration of the added TMB occurs. By comparing the colorimetric responses of TMB in Steps (1) and (2), the concentration of specific **PFAS** can be quantified. This detection method has been actively investigated in recent years, and various nanozymes have been fabricated, including metal-organic frameworks (**MOFs**),[66-70] zeolitic imidazolate frameworks (**ZIFs**),[71] metal oxide clusters,[72] gold nanoclusters,[73] and supramolecular polymers.[74] These nanozymes can detect **PFOA** or **PFOS** (each as a single substance) in water (and in methanol, in some cases) within 1 h (without **SPE**), with **LOD** within the range of approximately 50–400 ppb. These materials were hardly affected by contaminants such as ions (e.g., Na^+, K^+, Cl^-) found in tap and river water, and surfactants with structures similar to specific **PFAS** (e.g., sodium dodecyl sulfate (SDS) and sodium dodecyl benzenesulfonate (SDBS)). Because this method evaluates changes in absorbance at the same wavelength, it is expected to be difficult to detect and identify between different types and concentrations of **PFAS** in the presence of multiple **PFAS**. Notably, nanozymes with improved reactivity toward specific **PFAS** and ROS generation capacity (e.g., perfluoroalkyl-functionalized **MOF** (**Fe_3O_4@MON-F@Ru**, **PCN-222(Fe)-3F**),[66, 70] copper(I)-carbonitride (**Cu-CN**),[75] and copper-substituted cobalt-based Prussian blue derivative nanoboxes (**CuCO-PBA NB**)[65]) have achieved improved **LOD** of approximately 6–7 ppb. Although the nanozyme structurally optimized to interact with specific **PFAS** by the introduction of perfluoroalkyl chains prone to F-F interactions and cavity structures that increase specific surface area[65, 66, 70, 75] have made substantial progress toward achieving unprecedented ppt-level **LOD** in the colorimetric detection of specific **PFAS**, their application is limited by a complicated reaction process involving multiple reagents (an example reaction procedure is as follows: after incubating the nanozyme dispersion and **PFAS** aqueous solution for several tens of minutes, treat with TMB solution, which is reactive to ROS. the treated solution is reacted with incubation intervals of several tens of minutes, and its absorbance is measured at predetermined time points.) These materials were affected by competitive adsorption involving some ions that easily coordinates with the terminal groups (e.g., -COOH, -SO_3H) of specific **PFAS**, such as Cu^{2+} and SDS, as well as surfactants with structures similar to specific **PFAS**. Due to ROS generated on the nanozyme surface being involved in detecting specific **PFAS**, further sensitivity improvements can be expected by performing **SPE** to remove contaminants such as ions and surfactants from these detection materials. Since the detection mechanism involves inhibiting ROS generation due to surface adsorption of **PFAS** onto the nanozyme, surface modifications with substituents capable of altering interactions with different type of **PFAS** (e.g., perfluoroalkyl chains with varying carbon chains lengths[76]) is potentially possible to detect and identify between different types and concentrations of **PFAS** under conditions where multiple **PFAS** coexist.

[3] Dye-based detection used dyes that can interact with specific **PFAS** at the nano-level (e.g., porphyrin derivatives with perfluoroalkyl chains that interact with **PFAS** *via* F-F interactions[76-78], and methylene green that forms ion pairs with **PFOS**[79]). Among these, a portable kit called **astkCARE™**, which uses a dye (ethyl violet) similar to the active substance in methylene blue, is currently undergoing verification research with a view to practical application. This detection method involves extracting the hydrophobic ion pairs formed between ethyl violet and specific **PFAS** into an organic solvent (e.g., ethyl violet), enabling quantitative determination of the specific **PFAS** based on the colour change of the dye (**Figure 3C**).[80, 81] Additionally, the degree of colour change in the hydrophobic ion pairs formed by **PFOA** or **PFOS** and ethyl violet allows for the

View Article Online
DOI: 10.1039/D5NR05521K

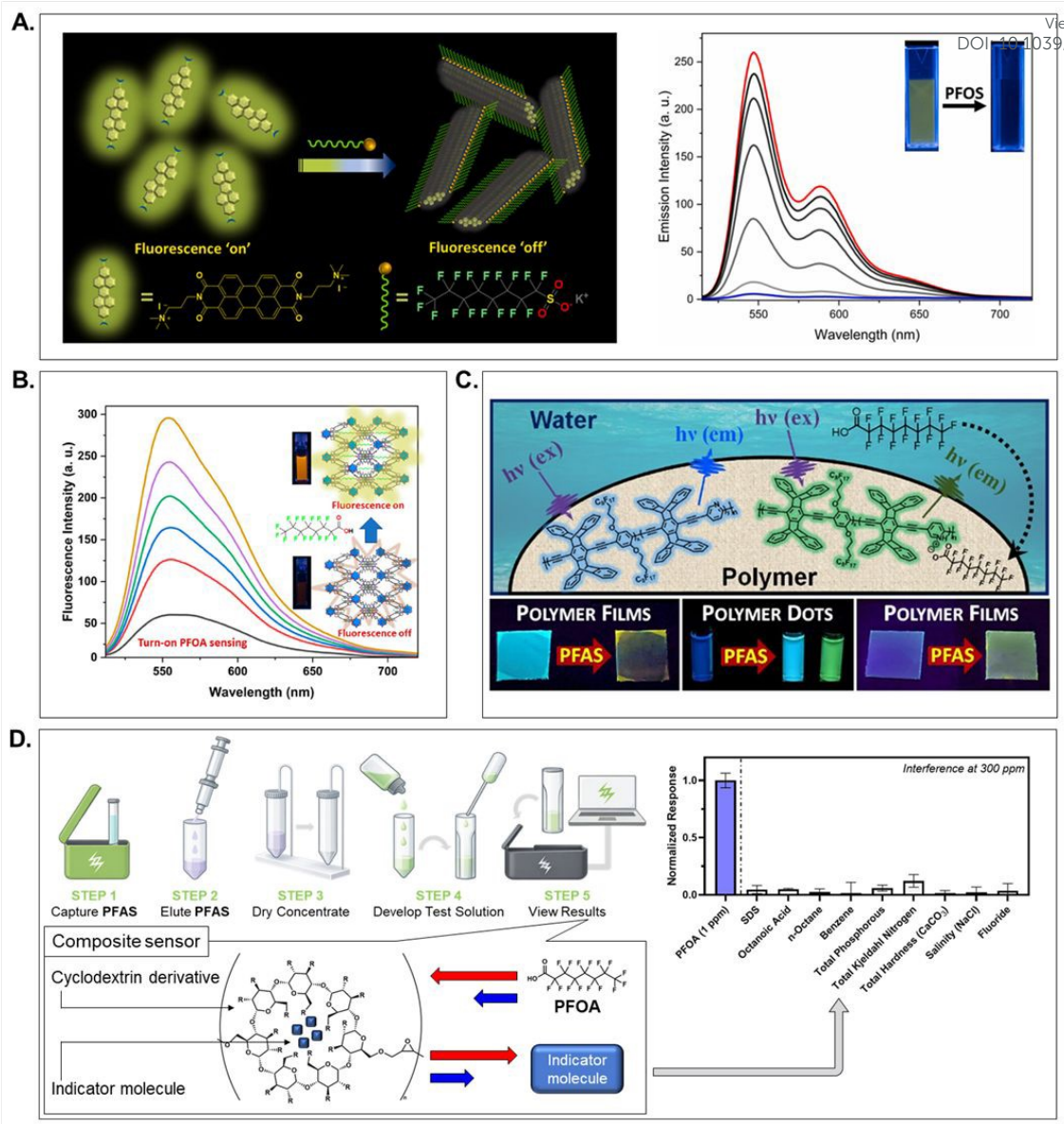

Figure 4 Schematic of the fluorescence detection of specific **PFAS**: Detection mechanism: (A) AIQ-induced quenching caused by specific **PFAS** coordination to material surface (turn-off type); (B) fluorescence induced by changes in the electronic environment caused by specific **PFAS** coordination on material surface (turn-on type); (C) change in fluorescence spectra owing to electron and energy transfer caused by specific **PFAS** coordination on material surface (ratiometric type); and (D) fluorescence changes of a composite sensor including cyclodextrin and indicator molecule with specific **PFAS** binding ability using **FRED-PFAS™**. Reproduced with permissions from ref. 84, Copyright 2025 Elsevier; refs. 86 and 92, Copyright 2023 and 2024 American Chemical Society; and ref. 59, Copyright 2025 National Ground Water Association.

separate detection of **PFOA** and **PFOS**. In this method, without **SPE**, the formation of coordination bonds with inorganic anions (primary constituents in tap water: Cl^-, SO_4^{2-}, others) was suggested, necessitating the removal of contaminants *via* **SPE** for enhanced sensitivity. However, **astkCARE™** still involves several issues, including ppb-level **LOD**, the need for **SPE** to achieve a low **LOD**, the use of organic solvents that are generally non-disposable during the dissolution of materials responsible for detecting specific **PFAS**, and long detection time (approximately 3 h) that includes **SPE**. Porphyrin derivative[76], featuring perfluoroalkyl chains with varying carbon chain lengths, has been reported to be able to control the type of **PFAS** susceptible to F-F interactions. This perfluoroalkyl chain has the following characteristics: (1) The hydrophobicity of the C-F bond site allows it to repel hydrocarbon contaminants such as dissolved organic matter.[82] (2) The low polarity and polarizability of the C-F bond site make it difficult to solvate ions, making it less susceptible to contaminants such as inorganic anions.[83] Therefore, optimizing the carbon chain length (hydrophobicity) of the perfluoroalkyl chain to match the carbon chain length of **PFAS** in the aqueous environments enables us to achieve selective detection of different types of **PFAS** from aqueous environments containing contaminants. Based on (1) and (2), introducing perfluoroalkyl chains of various carbon chain lengths into dyes such as ethyl violet enables us to potentially identify the target **PFAS** in aqueous environments where multiple **PFAS**, dissolved organic matters, and inorganic anions coexist. In contrast, since most

View Article Online
DOI: 10.1039/D5NR05521K

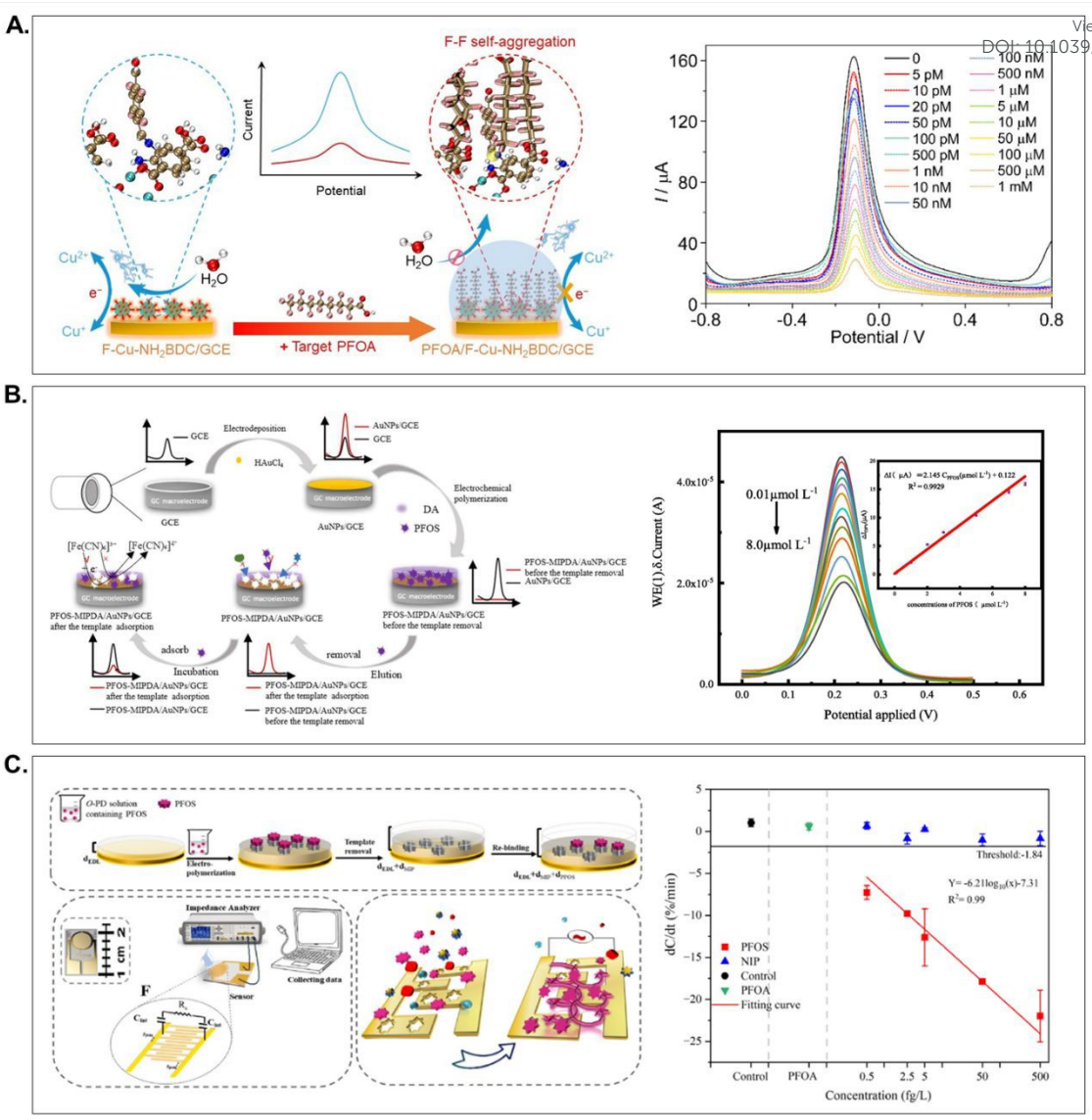

Figure 5 Schematic of electrochemical detection of specific **PFAS**: Detection mechanism: Adsorption of specific **PFAS** onto nanosized templates prepared on electrode surface by the electrolytic polymerization of (A) dopamine or (B) *o*-phenylenediamine; (C) Electrical signal enhancement using electrodes incorporating substances capable of interacting with specific **PFAS**. Reproduced with permissions from ref. 103 and 105, Copyright 2023 Elsevier; and ref. 106, Copyright 2025 American Chemical Society.

perfluoroalkyl chain-containing dyes are not water-soluble, **PFAS** cannot be detected directly in water; instead, detection and identification of **PFAS** must be performed in the organic solvent in which the dye is dissolved.

Based on [1]–[3], for practical application in on-site detection within actual aqueous environments, it is necessary to resolve issues such as the detection of specific **PFAS** at ppt levels, which is the regulatory value, the identification of the target **PFAS** in aqueous environments where multiple **PFAS** and contaminants exist based on differences in absorbance and absorption wavelength of detection materials, and the use of **SPE** and organic solvents.

2.2. Fluorescence detection

The detection of specific **PFAS** using fluorescent and quenching materials relies on changes in fluorescence intensity and wavelength that occur when the environment around the detection material changes owing to nano-level interactions with specific **PFAS**. These methods can be divided into three types: [1] 'turn-off type,' in which the fluorescence intensity decreases upon the adsorption or binding of specific **PFAS** to the material surface; [2] 'turn-on type,' in which the fluorescence intensity increases; and [3] 'ratiometric type,' in which the fluorescence spectrum shifts upon specific **PFAS** binding. The detection performance of these materials relies on electron and energy transfer at the material surface, where specific **PFAS** are present. By optimizing the type of detection material and its interaction with specific **PFAS**, highly sensitive

View Article Online
DOI: 10.1039/D5EN00524K

and selective detection of specific **PFAS** has been achieved, with **LOD** at the ppt–ppb level.

[1] In 'turn-off type' detection, **PFAS** form aggregates by coordinating with the surface of fluorescence material through electrostatic and hydrophobic interactions, causing aggregation-induced quenching (AIQ) (**Figure 4A**).[84] Perylene-diimide-based fluorescent sensors (**PDI-2+**, Dalapati *et al.*[84]) and aggregation-induced conjugated polymers (**FTD-MI**, Zhao *et al.*[85]) quantitatively measure the AIQ of **PFOA** or **PFOS** by coordinating them to the surface of materials, respectively. Detection of specific **PFAS** (**PFOA** or **PFOS**, respectively) in these materials have achieved **LOD** of 0.32–1.9 ppb within approximately 1 min (without **SPE**) in water or in water/dimethyl sulfoxide (DMSO) mixed solution, with minimal influence of contaminants such as ions (e.g., Na^+, K^+, Cl^-) found in tap and river water, and surfactants with structures similar to specific **PFAS** (e.g, SDS and SDBS). To evaluate changes in fluorescence intensity at same wavelength, these detection materials are expected to face difficulties in detecting and identifying each **PFAS** individually when multiple **PFAS** coexist. Furthermore, this method cannot completely eliminate the influence of background light from the detector during fluorescence measurements, making it necessary to exercise caution when interpreting small spectral changes.

[2] In 'turn-on type' materials, specific **PFAS** alter the electronic environment on the material surface, suppressing non-radiative quenching and increasing the fluorescence intensity of the detection material (**Figure 4B**)[86]. Dalapati *et al.* synthesized **Zr-MOF** (**U-1**)[86] incorporating hydrophobic perylene imide and a bifunctional **MOF** (**UiO-66-N(CH_3)$^{3+}$**).[87] In the case of **U-1**, the fluorescence intensity increased within 30 min (without **SPE**) in water or in water/organic solvent (DMSO or acetonitrile (MeCN)) mixed solution owing to the 'relaxation of π–π interactions *via* **PFOA** trapping within pores.' In contrast, **UiO-66-N(CH_3)$^{3+}$** exhibited increased intensity *via* 'ion exchange between anionic dyes adsorbed on the material surface and **PFOA**,' demonstrating a **LOD** of approximately 100–700 ppb. These materials were hardly affected by contaminants such as dissolved organic matter (e.g., lauric acid) present in tap water or river water, or surfactants with structures similar to specific **PFAS** (e.g., SDS and hexadecyltrimethylammonium bromide (CTAB)). To evaluate changes in fluorescence intensity at the same wavelength, these detection materials are expected to face difficulties in detecting and identifying each **PFAS** individually under the coexistence of multiple **PFAS**. Hassan *et al.* developed a hexanuclear cerium oxocluster (**[$Ce_6(\mu_3\text{-}O)_4(\mu_3\text{-}OH)_4$]$^{12+}$**) that exhibits aggregation-induced emission (AIE) upon interaction with **PFAS** and F-F bonds.[88] **[$Ce_6(\mu_3\text{-}O)_4(\mu_3\text{-}OH)_4$]$^{12+}$** was able to effectively quantify low concentrations of **PFOA** (**LOD**: 0.24 ppb) and **PFNA** (**LOD**: 0.4 ppb) within 10 min (without **SPE**) in water, and different types of **PFAS** such as also **PFHxA** and **PFDA** could be detected from each other based on the change in fluorescence of the materials. This material was unaffected by ionic contaminants (e.g., Na^+, K^+, Cl^-) found in tap and river water. Xu *et al.* synthesized a Tb(III) coordination polymer (**{Tb(L)(NO_3)(H_2O)$_2$}$_n$**) that displays AIE upon electrostatic interaction with specific **PFAS**, achieving **PFOA** detection at ultra-low concentrations within 10 min (without **SPE**) in water (**LOD**: 27.3 ppt) and unaffecting by interfering ions or surfactants.[89] **{Tb(L)(NO_3)(H_2O)$_2$}$_n$** was unaffected by contaminants such as ions (e.g., Na^+, K^+, Cl^-) present in tap water or river water, or surfactants (e.g, SDS and SDBS) with structures similar to specific **PFAS**. For evaluation of changes in fluorescence intensity at the same wavelength, these detection materials are also expected to face difficulties in detecting and identifying each **PFAS** individually in the presence of multiple **PFAS**. A composite (**SA hydrogel-N,F-CD composite**) formed by encapsulating fluorinated carbon dots (**F-CD**) in alginate hydrogel increased luminescence quantum yield by confining **PFOA** within the nanoscale space *via* F-F interactions between **F-CD** and **PFOA**. Although this system was noted to achieve ultra-high-sensitivity detection about 1 h (without **SPE**) in water (**LOD**: 0.001 ppt), it also exhibited slight fluorescence due to F-F interaction against the contaminant (NaF).[90, 91] The detection mechanism of this composite relies on F-F interactions with **PFAS** in nanoscale space, enabling enhanced selectivity for specific **PFAS** detection through removal of contaminants (NaF) using **SPE**. Similar to other 'turn-off type' detection materials, all detection materials for 'turn-on type' are expected to have difficulty detecting and identifying individual **PFAS** in the presence of multiple **PFAS**, as they evaluate changes in fluorescence intensity at a single wavelength.

[3] The 'ratiometric type' quantifies specific **PFAS** by analysing the intensity ratio of fluorescence wavelengths before and after the specific **PFAS** interact with the detection material, offering improved performance in complex aqueous environments (**Figure 4C**)[92]. Lanthanide **MOF**-based surface molecularly imprinted polymer probes (**Eu/Tb-MOF@MIPs**, Yang *et al.*[93]), were noted to amplify fluorescent polymers (**PPE-Py***, Concellón *et al.*[92]), and probes combining molybdenum boride (**MoB**) quantum dots (**QD**) with **N,F-CD** (**MoB QD/N,F-CD**, Wang *et al.*[94]) enabled **PFOA** detection in water (without **SPE**) (**LOD**: 0.1–40.6 ppb). Some materials were affected by ions (e.g., Fe^{2+}, Fe^{3+}) that readily coordinate with the terminal functional groups of specific **PFAS**. Due to the interaction between surfaces of material and specific **PFAS** being involved in the detection mechanism, the selectivity for detecting specific **PFAS** is expected to improve by removing contaminants using **SPE**. Based on the intensity ratio of different fluorescence wavelengths, these materials may enable detection and identification of **PFAS** types and concentrations in the presence of multiple **PFAS**. These methods primarily relied on changes in the ratio of two fluorescence intensities induced by binding to **PFOA** *via* F-F and electrostatic interactions. Donor-acceptor conjugated polymers (**PF-DBT-Im**, Chen *et al.*[95]) and aggregation-induced conjugated polymers (**FTD-C8-MI**, Zhao *et al.*[85]) incorporate structures exhibiting both fluorescence resonance energy transfer (FRET) and AIE within the same backbone. These detection materials enable the quantification of **PFOA** and **PFOS** present in water at the ppb level within several minutes (without SPE) based on the change in fluorescence by altering FRET through electrostatic or hydrophobic interactions with specific **PFAS** (**LOD**: 0.32–7.15 ppb). Several materials[94, 95] are affected by contaminants (e.g.,

View Article Online
DOI: 10.1039/D5NR05521K

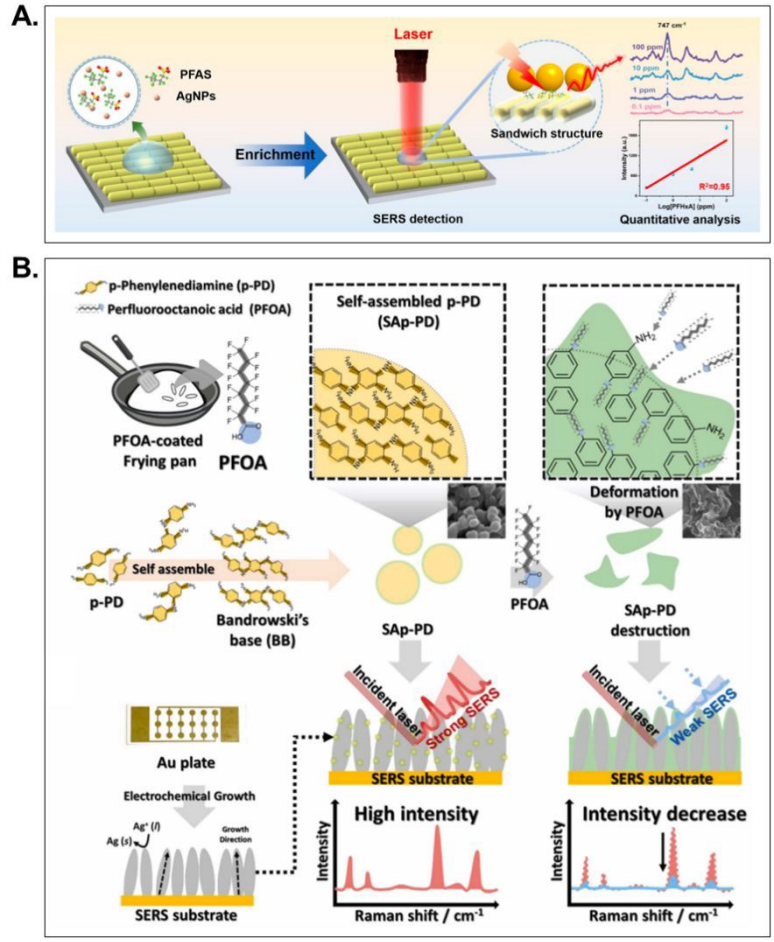

Figure 6 Schematic of the **SERS** detection of specific **PFAS**: Detection mechanism: (A) Enhancement of Raman signal by sandwiching specific **PFAS** with **Au NPs** and **Ag NPs**, (B) Enhancement of Raman signal using **Ag NPs** modified with substances capable of interacting with specific **PFAS**. Reproduced with permissions from ref. 109, Copyright 2023 American Chemical Society; and ref. 111, Copyright 2023 Elsevier.

SO_4^{2-}, NO_3^-, Cl^-, hydroquinone (HQUI), SDS, and SDBS) that promoted the aggregation of detection materials involved in the fluorescence energy transfer through electrostatic, hydrophobic, and π-π interactions. By improving the dispersion stability of the detection material using surfactants that are structurally dissimilar to **PFAS** (and do not impair interactions with **PFAS**), it is considered possible to prevent aggregation of the detection material caused by contaminants. Similar to other 'ratiotometric' detection materials, based on the intensity ratio of different fluorescent wavelengths for detection of **PFAS**, this method enables the detection and identification of **PFAS** species and concentrations even in the presence of multiple **PFAS**.

In terms of on-site detection of **PFAS** using fluorescent materials, verification research of **FRED-PFAS™**, a composite sensor consisting of a **CD** derivative capable of binding to specific **PFAS** and an indicator molecule (dye), are underway (**Figure 4D**).[59, 96, 97] The portable **FRED-PFAS™** can detect **PFOA** at the ppb–ppm level in organic solvent (methanol) and showed no response to Cl^-, CO_3^{2-}, or surfactants like SDS, though it faces several challenges, such as insufficient performance at the ppt level, undifferentiable from **PFAS** (Fluorotelomers and Aqueous Film-Forming Foam) other than **PFOA**, the need for **SPE** to achieve a low **LOD**, the use of methanol that are generally non-disposable during the dissolution of materials responsible for detecting specific **PFAS**, and long detection time (approximately 4 h) that includes **SPE**. Additionally, since **FRED-PFAS™** is a detection technology based on changes in fluorescence intensity at same wavelength, it is expected to be difficult to detect and identify the target **PFAS** from aqueous environments where multiple **PFAS** coexist.

Considering these findings, on-site detection of specific **PFAS** in actual aqueous environments requires overcoming challenges such as detection of specific **PFAS** at ppt levels in water containing contaminants, identification of the target **PFAS** in water containing multiple **PFAS** and contaminants due to differences in the fluorescence intensity and wavelength of the detection material, and the use of **SPE** and organic solvents.

2.3. Electrochemical detection

PFAS are electrochemically inactive and cannot be oxidized or reduced. Therefore, direct electrochemical detection of specific **PFAS** is generally not possible, and indirect strategies that enhance sensitivity are required. These approaches promote nano-level interfacial reactions between the electrode surface and specific **PFAS** to detect the target substance as an

View Article Online
DOI: 10.1039/D5NR05251K

electrical signal. Representative technologies include [1] fabrication of electrodes incorporating nanostructures that can interact with specific **PFAS**, and [2] nanosized template synthesis of specific **PFAS** on the electrode surface. By improving the electron-transfer properties of the electrode surface and adsorption of specific **PFAS** at the interface, high-sensitivity electrochemical detection at the ppt–ppb level can be realized. On the other hand, for stable specific **PFAS** detection, a supporting electrolyte such as phosphate-buffered saline (PBS) must be used in all electrochemical measurements.

[1] In the context of nanostructured electrodes, Shanbhag *et al.* fabricated a graphene-based electrode (**G/CPE**) with high adsorption capacity for specific **PFAS** owing to its high specific surface area.[98] **G/CPE** can quantify changes in electrical signals resulting from interactions between graphene π-electrons and specific **PFAS**, and was able to instantly detect **PFOA** (**LOD**: 4.31 ppb) and **PFDA** (**LOD**: 8.53 ppb) using PBS as the supporting electrolyte (without **SPE**). Nevertheless, this detection material was noted to be reactive toward contaminants, such as Zn^{2+}, Ni^{2+}, HQUI, which are likely to compete for adsorption through interactions similar to those of **PFAS** (e.g., electrostatic and hydrophobic interactions). To this end, removal of contaminants using **SPE** is recommended prior to detecting specific **PFAS**. Since this electrode cannot identify interactions based on the slight structural differences between various **PFAS**, detecting and identifying each **PFAS** in the presence of multiple **PFAS** is expected to be difficult. **Au NPs,**[99-101] silver nanoparticles (**Ag NPs**),[102] and copper-incorporated nanostructures (**F-Cu-NH_2BDC**, Zheng *et al.*[103]; **Cu@CuO aerogel**, Xu *et al.*[104]) with excellent electron transfer properties have been for highly sensitive detection of **PFAS** (**Figure 5A**),[103] In general, the surfaces of **Au NPs** or **Ag NPs** can be functionalized with substances capable of interacting with specific **PFAS**, such as dyes (**MB@AuNPs**, Simonetti *et al.*[99]), perfluoroalkyl chains (carbon chain length of 8 or more) (**PFTD/AuNPs/GCE**, Calvillo Solís *et al.*[100]), citrate (**MXene-AgNPs**,[102]), and nickel oxide (**AuNPs/NiOScZ/SPCE**, Comnea-Stancu *et al.*[101]). These materials were able to quantify trace amounts of **PFAS** (perfluorobutanoic acid (**PFBA**), **PFOA**, **PFOS**, perfluoroundecanoic acid (**PFUnDA**), each a single substance) within 1 h using PBS or $KHCO_3$ as the supporting electrolyte (without **SPE**) (**LOD**: 0.033–24.0 ppt). However, it was revealed that electrochemical reactivity toward contaminants such as Mg^{2+}, Na^+, which readily coordinate with the terminal functional groups of specific **PFAS**, as well as SDS and SDBS, which have structures similar to specific **PFAS**, and that the selectivity for **PFAS** detection was low. In detection technologies of [1], while these materials have the advantage of detecting ppt-level specific **PFAS** through electrostatic interactions or hydrophobic interactions between the electrode and the specific **PFAS**, the interaction between the material surface and the specific **PFAS** significantly influences the detection mechanism; consequently, they are susceptible to interference from inorganic anions and surfactants, and have the limitation necessitating the contaminant removal step using **SPE**. These materials, by surface-modifying substances with varying abilities to interact with various **PFAS** (e.g., perfluoroalkyl chains with varying carbon chains lengths (3–12)[76], may enable detection and identification tailored to the type and concentration of **PFAS** even in the presence of multiple **PFAS**.

[2] In nanosized template synthesis, electrolytic polymerization of dopamine or *o*-phenylenediamine occurs on the electrode surface in the presence of **PFOS** (**Figure 5B, 5C**).[105-108] The binding of **PFOS** to the nanosized template can be detected as a change in electrical signal. Sensors fabricated by Amin *et al.* (**molecularly imprinted poly *o*-PD on Au interdigitated microelectrodes**)[106] and Lu *et al.* (**MIP/AuNS/GCE**)[108] achieved ppt-level **LOD** within minutes (without **SPE**). Some of these materials demonstrate high detection sensitivity for **PFOS** among **PFAS** species (perfluoropentanoic acid (**PFPA**), perfluoroheptanoic acid (**PFHpA**), and **PFOA**, each as a single substance) under conditions using PBS as the supporting electrolyte. Nevertheless, the sensitivity to some contaminants such as Na^+, Cl^-, and humic acid, which are likely to competitively adsorb to the electrode surface through similar interactions (e.g., electrostatic and hydrophobic interactions) as **PFAS**, have been reported.[108] The methods to enhance the detection sensitivity and selectivity of this electrode for specific **PFAS** include removing contaminants *via* **SPE** and surface modification of the electrode using substituents that readily interact with **PFAS**. In detection technologies of [2], these materials have the advantage of controlling the detection sensitivity for **PFOS** and other **PFAS** through nanosized templates fabricated on the electrode surface using **PFOS**. On the other hand, the nanosized template synthesis for different types of **PFAS** (especially those with short carbon chains) is challenging (due to weak interactions between the monomers used in electrolytic polymerization and **PFAS** with short carbon chains), and they are susceptible to competitive adsorption with inorganic anions and surfactants on the material surface, and have the limitation necessitating a process for removing contaminants using **SPE**. Therefore, by applying the methods described in [1] (incorporation of nanostructures and surface modification of substituents that easily interact with **PFAS**) to electrodes equipped with nanosized templates, it is potentially possible to detect and identify between different types and concentrations of **PFAS** in the presence of multiple **PFAS** without **SPE**.

From [1]–[2], to apply this technology to on-site detection in actual aqueous environments, it is necessary to resolve issues such as installation of equipment for electrochemical detection in a wide area (ensuring a stable power source and preparing the optimal supporting electrolyte for each water body), selective detection of **PFAS** in the presence of contaminants, and identification of the target **PFAS** in aqueous environments where multiple **PFAS** exist due to differences in potential.

2.4. SERS detection

SERS is a powerful spectroscopic technology capable of detecting molecule-specific vibrational spectra. For ultra-low concentration analysis of specific **PFAS** using **SERS**, the selection of a substrate capable of enhancing Raman signals and the immobilization of specific **PFAS** onto the substrate are critical.

View Article Online
DOI: 10.1039/D5NR02523K

Typically, substrates are coated with **Ag NPs** that provide electromagnetic enhancement *via* localized surface plasmon resonance. To detect changes in Raman signals based on the presence of specific **PFAS** on the substrate, two approaches have been designed: [1] sandwiching specific **PFAS** between **Ag NPs** and **Au NPs**, and [2] adding or modifying materials to the **Ag NPs** surface to facilitate specific **PFAS** immobilication.

[1] Feng *et al.* deposited a mixture of **Ag NPs** and **PFAS** onto a substrate containing **Au NPs**, allowing the **PFAS** to be sandwiched between the **Ag NPs** and **Au NPs** after drying (**Figure 6A**).[109] This sandwich method enabled the identification of **PFHxA**, **PFOA**, and **PFBS** in water based on slight differences in the Raman signal peak positions, with an **LOD** values of 100 ppb for each (without **SPE**). The effect assessment of contaminants on this method had been untested. Identification of **PFAS** using this method relies on slight differences in the peak positions of Raman signals originating from structurally similar types of **PFAS**; hence, in the presence of multiple **PFAS**, peak position shifts are expected to occur competitively in principle, making detection and identification based on **PFAS** types and concentrations difficult.

[2] Kumar *et al.* added malachite green, which forms ion pairs with specific **PFAS**, to increase the affinity between **Ag NPs** on a substrate and specific **PFAS**.[110] This method enabled the rapid quantification of **PFOS** in water, with an **LOD** of 49.1 ppb. In addition, there was no effect from contaminants contained in soil and lake water, and urine (e.g., major components in soil and lake water: Cl^-, SO_4^{2-}, humic acid; major components in urine: Na^+, K^+, Cl^-, SO_4^{2-}, urea). Due to the high affinity between **Ag NPs** on this **SERS** substrate and different types of **PFAS**, the slight differences in the peak positions of Raman signals from different types of **PFAS** are expected to become easier to recognize. Nevertheless, under conditions where multiple **PFAS** of different types with highly similar structures coexist, shifts in the peak positions of Raman signals can also occur due to competition in principle, making detection and identification based on **PFAS** type and concentration difficult. To support the immobilization of specific **PFAS** onto substrates, **Ag NPs** have been surface-modified with *p*-phenylenediamine nanoparticles (Park *et al.*[111]), thiol molecules (Rothstein *et al.*[112]), graphene (McDonnell *et al.*[113]), and **CD** (Li *et al.*[114]), which can interact with specific **PFAS** (**Figure 6B**). On this **SERS** substrate containing **Ag NPs**, changes in Raman signals before and after the addition of **PFOA** or **PFOS** in water (and in methanol, in some cases) could be immediately detected and identified, achieving an **LOD** of 0.4–40 ppt. The **SERS** substrate[111]

Table 1 Summary table of **PFAS** detection by colorimetric technology. Interfering species of each research were excerpted from representative ions, surfactants, dissolved organic matter, among others. "–" indicates that "**Selectivity**" column was "Untested". "Good" in the "**Selectivity**" column indicates that the detection material did not show significant changes to the interfering species tested in that research. (The abbreviation is as follows: **PFHxA**: perfluorohexanoic acid; **PFOA**: perfluorooctanoic acid; **PFNA**: perfluorononanoic acid; **PFDA**: perfluorodecanoic acid; **PFOS**: perfluorooctanesulfonic acid; **PFOPA**: 1H,1H,2H,2H-perfluorooctanephosphonic acid; **SPE**: solid-phase extraction; DMF: *N*,*N*-dimethylformamide; MeOH: methanol; EtOAc: ethyl acetate; SDS: sodium dodecyl sulfate; SDBS: sodium dodecylbenzene sulfonate; SOS: sodium octyl sulfate; CTAB: cetyltrimethylammonium bromide; CTAC: cetyltrimethylammonium chloride; PVP: polyvinylpyrrolidone)

Detection Method	Material	Analytes	LOD	Detection Time	Measurement Solvent	Interfering Species	Selectivity	Detection Mechanism	Ref.
Colorimetric	CD@AuNPs	PFOA	70.4 ppb	60 min	Water/DMF	Environmental water samples	Good	Aggregation due to **PFAS** adsorption on the surface of **Au NPs**	63
	Citrate-Au NPs	PFHxA PFOA PFNA PFDA PFOS PFOPA	42.7–2,005 ppb	1 s	Water	Cl^-, Na^+, Mg^{2+}, Suwanee river Dissolved organic matter, pH (4, 7, 10)	Affected by dissolved organic matter, ions (Cl^-, Mg^{2+}), pH (7, 10)		64
	CuCo-PBA NB	PFOS	7.15 ppb	30 min	Water	NO_3^-, SO_4^{2-}, CO_3^{2-}, Ac^-, HCO_3^-, HPO_4^{2-}, Ni^{2+}, Na^+, Al^{3+}, Cu^{2+}, Ba^{2+}, Fe^{2+}, Fe^{3+}, SDS, CTAB, PVP	Affected by ions (CO_3^{2-}, HCO^{3-}, Ba^{2+}), surfactants (SDS, CTAB, PVP)		65
	Fe_3O_4@MON-F@Ru	PFOS	7.70 ppb	50 min	MeOH	Cl^-, NO_3^-, SO_4^{2-}, Na^+, K^+, Fe^{2+}	Good		66
	F-Ce-UiO-66-NH_2	PFOA	169.8 ppb	40 min	Water	F^-, Cl^-, Br^-, NO_3^-, SO_4^{2-}, Na^+, K^+, Mg^{2+}, Cu^{2+}, Fe^{3+}, Zn^{2+}, Cr^{3+}, Pb^{2+}, NH_4^+, SDBS, PVP	Good		67
	Fe/Zn-BDC	PFOS	50.0 ppb	15 min	Water	F^-, Cl^-, Br^-, SO_4^{2-}, CO_3^{2-}, Na^+, K^+, Mg^{2+}, Ca^{2+}, PVP, CTAB, CTAC	Good		68
	MOFs derived Cu/C nanocomposite	PFOA	55.1 ppb	40 min	Water	Cl^-, SO_4^{2-}, HPO_4^{2-}, Ac^-, Cu^{2+}, Fe^{3+}, Na^+, SDS	Good	Inhibition of color reaction resulting from **PFAS** adsorption to surface of nanozyme catalyzing ROS generation	69
	PCN-222(Fe)-3F	PFOS	6.30 ppb	30 min	Water	Cl^-, SO_4^{2-}, CO_3^{2-}, HPO_4^{2-}, Ac^-, Na^+, K^+, Mg^{2+}, Ca^{2+}, Cu^{2+}, SDS, SOS, CTAB	Affected by surfactants (SDS, SOS, CTAB)		70
	MGO@ZIF-8@MIP	PFOA	49.7 ppb	50 min	Water	Na^+, K^+, Mg^{2+}	Good		71
	$[(CH_3)_2NH_2]V_3O_7$	PFOS	230.0 ppb	20 min	Water	Cl^-, Br^-, SO_4^{2-}, CO_3^{2-}, HPO_4^{2-}, Na^+, K^+, Mg^{2+}, Ca^{2+}, Zn^{2+}, Ni^{2+}, Mn^{2+}, SDS, CTAB, PVP, CTAC	Good		72
	AuNCs@CMP	PFOS	75.0 ppb	20 min	Water	Cl^-, SO_4^{2-}, Na^+, K^+, Mg^{2+}	Good		73
	SMIP@N-CF	PFOA	401.7 ppb	5 min	Water	–	Untested		74
	Cu-CN	PFOS	7.45 ppb	30 min	Water	SO_4^{2-}, CO_3^{2-}, $B_4O_7^{2-}$, HPO_4^{2-}, $H_2PO_4^-$, Ac^-, Na^+, Ca^{2+}, Cu^{2+}, Fe^{3+}, Fe^{2+}, SDS, SDBS, SOS, CTAB, PVP	Affected by surfactants (SDS)		75
	astkCARE™	PFOA PFOS	10 ppb (without SPE) 0.5 ppb (with SPE)	5 min (without SPE) 3 h (with SPE)	Water/EtOAc	Tap water, Ground water	Affected by inorganic ions in tap/ground water	Color change of a solution containing hydrophobic ion pairs formed by dyes and **PFAS**	80 81

View Article Online
DOI: 10.1039/D5NR03521A

Table 2 Summary table of **PFAS** detection by fluorescence technology. Interfering species of each research were excerpted from representative ions, surfactants, dissolved organic matter, among others. "**–**" indicates that "**Selectivity**" column was "Untested". "Good" in the "**Selectivity**" column indicates that the detection material did not show significant changes to the interfering species tested in that research. (The abbreviation is as follows: **PFHxA**: perfluorohexanoic acid; **PFOA**: perfluorooctanoic acid; **PFNA**: perfluorononanoic acid; **PFDA**: perfluorodecanoic acid; **PFOS**: perfluorooctanesulfonic acid; **6:2 FTS**: 6:2 fluorotelomer sulfonate; **AFFF**: aqueous film-forming foam; **SPE**: solid-phase extraction; DMF: *N*,*N*-dimethylformamide; MeOH: methanol; DMSO: dimethyl sulfoxide; MeCN: acetonitrile; EtOH: ethanol; SDS: sodium dodecyl sulfate; SDBS: sodium dodecylbenzene sulfonate; CTAB: cetyltrimethylammonium bromide; CTAC: cetyltrimethylammonium chloride; Tween-20: polyoxyethylene (20) sorbitan monolaurate; PEG-4000: polyethylene glycol 4000)

Detection Method	Material	Analytes	LOD	Detection Time	Measurement Solvent	Interfering Species	Selectivity	Detection Mechanism	Ref.
Fluorescence	**PDI-2+**	**PFOS**	1.9 ppb	1 min	Water	NO_3^-, HCO_3^-, $S_2O_3^{2-}$, PO_4^{3-}, Na^+, K^+, Mg^{2+}, Ca^{2+}, Fe^{3+}, Li^+, SDS, Lauryl sulfate, Lauric acid	Good	AIQ-induced quenching caused by **PFAS** coordination to material surface (Turn-off type)	84
	FTD-MI, FTD-C_8-MI	**PFOA** **PFOS**	**FTD-MI**: 1.18 ppb (**PFOA**) 0.32 ppb (**PFOS**) **FTD-C_8-MI**: 2.24 ppb (**PFOA**) 2.42 ppb (**PFOS**)	1 s	Water/DMSO	Cl^-, NO_3^-, SO_4^{2-}, CO_3^{2-}, HPO_4^{2-}, HSO_3^- Ac^-, Na^+, Cu^{2+}, Fe^{3+}, Mn^{2+}, Pb^{2+}, Bi^{3+}, Co^{2+}, Cd^{2+}, Ce^{2+}, CTAB, CTAC	Good		85
	U-1	**PFOA**	695.6 ppb	30 min	Water/DMF	CTAB, Lauric acid	Good		86
	UiO-66-N$(CH_3)^{3+}$	**PFOA**	91.1 ppb	40 min	Water/MeCN	SDS, Lauric acid	Good		87
	$[Ce_6(\mu_3\text{-}O)_4(\mu_3\text{-}OH)_4]^{12+}$	**PFHxA** **PFOA** **PFNA** **PFDA**	0.24 ppb (**PFOA**) 0.4 ppb (**PFNA**)	10 min	Water	F^-, Cl^-, I^-, CO_3^{2-}, PO_4^{3-}, Na^+, K^+	Good	Fluorescence due to changes in the electronic environment caused by **PFAS** coordination on material surface (Turn-on type)	88
	{Tb(L)$(NO_3)(H_2O)_2$}vv$_n$	**PFOA**	27.3 ppt	10 min	Water	F^-, Cl^-, NO_3^-, SO_4^{2-}, SCN^-, Na^+, Mg^{2+}, Fe^{2+}, NH_4^+, SDS, SDBS, CTAB	Good		89
	SA Hydrogel-N,F-CDs Composite	**PFOA**	0.001 ppt	60 min	Water	Cl^-, NO_3^-, $H_2PO_4^-$, Na^+, K^+, Ca^{2+}, Ni^{2+}	Good		90
	F-CD	**PFOA**	3.0 ppt	30 min	Water/EtOH	F^-, Cl^-, NO_3^-, HPO_4^{2-}, $H_2PO_4^-$, Na^+, K^+, Ca^{2+}, Fe^{3+}, Ni^{2+}	Affected by ions (F^-)		91
	PPE-Py[a]	**PFOA**	100 ppt	60 min	Water	–	Untested		92
	Eu/Tb-MOF@MIPs	**PFOA**	40.6 ppb	4 min	Water	F^-, Cl^-, NO_3^-, CO_3^{2-}, Na^+, K^+, Mg^{2+}, Ca^{2+}	Good		93
	MoB QDs and N, F-CDs	**PFOA**	4.14 ppb	4 min	Water	Cl^-, Br^-, NO_3^-, SO_4^{2-}, CO_3^{2-}, Na^+, K^+, Mg^{2+}, Cu^{2+}, Fe^{2+}, Fe^{3+}, Zn^{2+}, Mn^{2+}, Ba^{2+}, Al^{3+}, Cr^{3+}, NH^4, CTAB	Affected by ions (Br^-, Fe^{2+}, Fe^{3+}, Al^{3+}, Cr^{3+}), surfactants (CTAB)	Change in fluorescence spectra due to electron and energy transfer caused by **PFAS** coordination on material surface (Ratiometric type)	94
	PF-DBT-Im	**PFOA** **PFOS**	2.53 ppb (**PFOA**) 7.15 ppb (**PFOS**)	1 s	Water	Cl^-, I^-, SO_4^{2-}, CO_3^{2-}, Ac^-, $H_2PO_4^-$, Na^+, Mg^{2+}, Ca^{2+}, Cu^{2+}, Ba^{2+}, Fe^{2+}, Fe^{3+}, Zn^{2+}, Cr^{3+}, Co^{2+}, Ni^{2+}, Ag^+, Cd^{2+}, Pb^{2+}, Ce^{2+}, SDS, SDBS, CTAB, CTAC, Tween-20, PEG-4000	Affected by surfactants (SDS, SDBS)		95
	FRED-PFAS™	**PFOA** **6:2 FTS** **AFFF**	1 ppm (**PFOA**)	4 h (with **SPE**)	Water/MeOH	Cl^-, CO_3^{2-}, Na+, Ca^{2+}, SDS	Good	Fluorescence changes of the composite sensor of cyclodextrin and indicator molecule with **PFAS** binding ability	59 96 97

Table 3 Summary table of **PFAS** detection by electrochemical technology. Interfering species of each research were excerpted from representative ions, surfactants, dissolved organic matter, among others. "**–**" indicates that "**Selectivity**" column was "Untested". "Good" in the "**Selectivity**" column indicates that the detection material did not show significant changes to the interfering species tested in that research. (The abbreviation is as follows: **PFBA**: perfluorobutanoic acid; **PFPA**: perfluoropentanoic acid; **PFHpA**: perfluoroheptanoic acid; **PFOA**: perfluorooctanoic acid; **PFUnDA**: perfluoroundecanoic acid; PBS: phosphate buffered saline; MeOH: methanol; EtOH: ethanol; SDS: sodium dodecyl sulfate; SDBS: sodium dodecylbenzene sulfonate; CTAB: cetyltrimethylammonium bromide; PVP: polyvinylpyrrolidone; HQUI: hydroquinone; 4-DBS: 4-dodecylbenzenesulfonic acid)

Detection Method	Material	Analytes	LOD	Detection Time	Measurement Solvent	Interfering Species	Selectivity	Detection Mechanism	Ref.
Electrochemical	**G/CPE**	**PFOA** **PFDA**	4.31 ppb (**PFOA**) 8.53 ppb (**PFDA**)	1 s	PBS/EtOH	Cl^-, NO_3^-, SO_4^{2-}, CO_3^{2-}, Na^+, K^+, Mg^{2+}, Cu^{2+}, Fe^{2+}, Zn^{2+}, Ni^{2+}	Affected by ions (Cl^-, NO_3^-, SO_4^{2-}, K^+, Mg^{2+}, Fe^{2+}, Ni^{2+})		98
	MB@AuNPs	**PFBA** **PFUnDA** **PFOS**	2.7 ppt	150 s	PBS	Na^+, Ca^{2+}, SDS, CTAB, Tween-20	Affected by surfactants (SDS)		99
	PFTD/AuNPs/GCE	**PFOA**	24 ppt	120 s	$KHCO_3$ solution	–	Untested		100
	AuNPs/NiOScZ/SPCE	**PFOA**	12 ppt	1 s	PBS	NO_3^-, Na^+, K^+, Ca^{2+}, Cu^{2+}, Fe^{2+}, Mn^{2+}, HQUI	Good	Electrical signal enhancement using electrodes incorporating substances capable of interacting with **PFAS**	101
	MXene-AgNPs	**PFOS**	0.033 ppt	5 min	PBS	F^-, Cl^-, I^-, SO_4^{2-}, PO_4^{3-}, Na^+, K^+, Mg^{2+}, 4-DBS	Affected by surfactants (4-DBS)		102
	F-Cu-NH_2BDC	**PFOA**	1.47 ppt	1 s	PBS	Na^+, K^+, Mg^{2+}, Cu^{2+}, Fe^{3+}, Zn^{2+}, Pb^{2+}, Co^{2+}, Cr^{3+}, Ni^{2+}, SDS, SDBS, CTAB	Good		103
	Cu@CuO aerogel	**PFOS**	1.65 ppb	30 min	PBS	Na^+, K^+, Mg^{2+}, Ca^{2+}, Mn^{2+}, Cd^{2+}, Ce^{2+}, SDS, SDBS, PVP	Affected by ions (Mn^{2+}), surfactants (SDS, SDBS, PVP)		104
	PFOS-MIPPDA/AuNPs/GCE	**PFOS**	2.1 ppb	15 min	PBS	Cl^-, SO_4^{2-}, CO_3^{2-}, SiO_3^{2-}, Na^+, K^+, Mg^{2+}, Ca^{2+}, Ba^{2+}, NH_4^+	Good		105
	Molecularly imprinted Poly *o*-PD preparation on Au-IDMEs	**PFPA** **PFHpA** **PFOA** **PFOS**	0.0005 ppt (**PFOS**)	10 s	PBS	–	Untested	Adsorption of **PFAS** onto nanosized templates prepared on electrode surface	106
	CNW/MIP	**PFOS**	1.2 ppb	12 min	PBS	–	Untested		107
	MIP/AuNS/GCE	**PFOS**	7.5 ppt	10 min	PBS/MeOH	Cl^-, Na^+, Humic acid	Affected by ions (Cl^-)		108

View Article Online DOI: 10.1039/D5NR03921A

Table 4 Summary table of **PFAS** detection by **SERS** technology. Interfering species of each research were excerpted from representative ions, surfactants, dissolved organic matter, among others. "–" indicates that "**Selectivity**" column was "Untested". "Good" in the "**Selectivity**" column indicates that the detection material did not show significant changes to the interfering species tested in that research. (The abbreviation is as follows: **PFHxA**: perfluorohexanoic acid; **PFOA**: perfluorooctanoic acid; **PFBS**: perfluorobutanesulfonic acid; **PFOS**: perfluorooctanesulfonic acid; MeOH: methanol)

Detection Method	Material	Analytes	LOD	Detection Time	Measurement Solvent	Interfering Species	Selectivity	Detection Mechanism	Ref.
SERS	Au@AgNRs	PFHxA PFOA PFBS	100 ppb	1 s	Water	–	Untested	Enhancement of raman signal by sandwiching **PFAS** with **Au NPs** and **Ag NPs**	109
	AgNPs on fish scale substrates	PFOS	49.1 ppb	1 s	Water	Lake water, Soil, Urine samples	Good		110
	Self-assembled *p*-phenylenediamine (SAp-PD) nanoparticles	PFOA	0.53 ppt	1 s	Water	Tap water, Oxalic acid, Citric acid, Succinic acid	Good		111
	AgNR substrate	PFOA PFOS	1 ppt (**PFOA**) 4.28 ppb (**PFOS**)	1 s	MeOH	–	Untested	Enhancement of raman signal using **Ag NPs** modified with substances capable of interacting with **PFAS**	112
	Graphene and Ag NPs printed on kapton substrate	PFOA PFOS	0.40 ppt	1 s	Water	–	Untested		113
	β-CD/Ag Nanocomplexes in the Microstructured Optical Fiber	PFOA	40 ppt	1 s	Water	–	Untested		114

containing **Ag NPs** surface-modified with *p*-phenylenediamine nanoparticles could instantly detect and identify changes in the peak positions of Raman signals before and after addition of **PFOA** in water, achieving the **LOD** of 0.53 ppt. The reactivity toward inorganic anions (primary constituents in tap water: Cl^-, SO_4^{2-}, others) was evaluated, though it had minimal impact on the detection of specific **PFAS**. The **Ag NPs** on this **SERS** substrate are readily interacted with different types of **PFAS**, making it easier to recognize the slight differences in the peak positions of Raman signals from different **PFAS**. On the other hand, under conditions where multiple **PFAS** of different types with similar structures coexist, shifts in the peak positions of Raman signals are also expected to occur due to competition in principle, making detection and identification based on **PFAS** type and concentration difficult. **SERS** substrates containing thiol molecules[112], graphene[113], and **CD**[114]-surface-modified **Ag NPs** could instantly detect and identify changes in the peak positions of Raman signals before and after addition of **PFOA** or **PFOS** in water (some in methanol), with **LOD** ranging from 0.4–40 ppt. The effect of contaminants on these **SERS** substrates had not been evaluated. The **Ag NPs** on these **SERS** substrates also interact readily with each type of **PFAS**, making it easier to recognize the slight differences in the peak positions of Raman signals from different **PFAS**. Nonetheless, under conditions where multiple structurally similar **PFAS** coexist, shifts in the peak positions of Raman signals are also expected to occur due to fundamental competition, making detection and identification based on **PFAS** type and concentration difficult.

In many cases, the effects of contaminants (e.g., ions, surfactants, and dissolved organic matter) on detection performance remain to be clarified. Besides, there are fewer examples of detection and identification of **PFAS** species other than **PFOA** and **PFOS** compared to other studies. These research, based on slight differences in the peak positions of Raman signals corresponding to different type of **PFAS** with highly similar structures, indicate that under conditions where multiple **PFAS** coexist, shifts in the peak positions of Raman signals can also occur due to competition; therefore, while further consideration is necessary, it is highly possible that detection and identification will become difficult depending on the type and concentration of **PFAS**. To apply this method for on-site detection in actual aqueous environments, it is necessary to verify changes in the peak positions of Raman signals under conditions where various **PFAS** are present, as well as the feasibility of identifying target **PFAS** from aqueous environments containing multiple **PFAS** and contaminants.

3. Conclusion

Although regular monitoring of specific **PFAS** in aqueous environments is being prioritized worldwide, LC-MS/MS remains the only technique capable of detecting and identifying specific **PFAS** at the ppt level. However, LC-MS/MS is expensive, time-intensive, and inaccessible to non-experts, rendering it unsuitable for assessing potentially contaminated water sources. This review outlines rapid and sensitive detection research based on nano-level interaction with specific **PFAS** that can overcome the challenges of LC-MS/MS. Detection methods for specific **PFAS** can be divided into **2.1. Colorimetric**, **2.2. Fluorescence**, **2.3. Electrochemical**, and **2.4 SERS**-based methods. The corresponding detection mechanisms and optimization methods to improve detection sensitivity, along with **LOD** values are summarized (**Table 1: Colorimetric**, **Table 2: Fluorescence**, **Table 3: Electrochemical**, **Table 4: SERS**). These detection research enable the detection of specific **PFAS** in a short time (within several minutes to hours) compared with LC-MS/MS, which requires half a day – more than a day of measurement time. However, among the major specific **PFAS** detection research summarized, few have been able to detect levels of several ppt in actual aqueous environments. Furthermore, due to challenges such as undesirable reactions and interactions caused by contaminants, as well as the difficulty of detecting and identifying only the target **PFAS** in aqueous environments with varying pH levels where multiple **PFAS** and contaminants coexist; consequently, most research based on nano-level interactions with specific **PFAS** has not advanced to verification research for use in actual on-site detection (selective detection of specific **PFAS** at several ppt levels in aqueous environments with different pH levels containing contaminants such as ions and dissolved organic matter).

View Article Online
DOI: 10.1039/D5NR00652H

4. Future prospects for detection research based on nano-level interactions

While diverse technologies based on nano-level interactions are being explored for detecting trace specific **PFAS**, each method faces specific challenges. **2.1. Colorimetric detection** of specific **PFAS** was performed primarily in water (without **SPE**) and was able to detect **PFOA**, **PFOS**, and other **PFAS** at levels of several ppb–ppm level; however, this method has not achieved detection of **PFAS** at regulatory levels (several ppt level) established in countries worldwide. For this reason, it is urgent to achieve the **LOD** at the ppt level for **PFAS**-responsive dyes by combining surface modification with substituents that enhance interactions with **PFAS** (e.g., perfluoroalkyl chains capable of F-F interactions[76] and quaternary ammonium groups enabling electrostatic interactions[115]) and expansion of the **PFAS**-responsive site (e.g., introduction of cavity structures or increasing specific surface area through porosity). Due to the influence of contaminants such as ions found in tap water or river water and surfactants with structures similar to specific **PFAS**, some detection materials recommend removing contaminants *via* **SPE** prior to detection of **PFAS**. Based on the evaluation of changes in absorbance and absorption spectrum at same wavelength, this research is expected to be difficult to detect and identify different type and concentration of **PFAS** in the presence of multiple **PFAS**. Research on **2.1. Colorimetric detection** for on-site detection (with **SPE**) is also underway, and **PFOA** or **PFOS** were successfully detected based on the colour tones of the hydrophobic ion pairs formed between the extracted **PFOA** or **PFOS** and a dye in ethyl acetate. However, even with prolonged **SPE**, contaminants cannot be completely removed, making it impossible to detect specific **PFAS** at the ppt level. Furthermore, it necessitates the use of ethyl acetate that cannot be disposed of as general waste when detecting specific **PFAS**. By introducing perfluoroalkyl chains[76] of varying carbon chain lengths capable of identifying different types of **PFAS** into dyes used for **2.1. Colorimetric detection** verification research, it is potentially possible to suppress reactivity with inorganic anions and achieve identification of target **PFAS** in aqueous environments where multiple **PFAS** coexist. However, many dyes incorporating perfluoroalkyl chains are not water-soluble, making it impossible to directly detect **PFAS** in water; therefore, detection and identification of **PFAS** must be performed in organic solvents where the dyes are soluble.

2.2 Fluorescence detection enables highly sensitivity detection of **PFOA**, **PFOS**, and other **PFAS** at the ppt–ppb levels, primarily in water (without **SPE**) compared to **2.1. Colorimetric detection**. This method showed **LOD** for **PFAS** detection that are close to regulatory levels (several ppt level) set around the world. However, for detection materials with **LOD** close to the ppt level, the quantitation capabilities of specific **PFAS** tend to be compromised due to the influence of ions that readily coordinate with the terminal functional groups of specific **PFAS** found in tap water or river water, as well as contaminants from surfactants with structures similar to specific **PFAS**. Therefore, it is necessary to remove contaminants that reduce the quantification abilities of specific **PFAS** using **SPE**, and the formation of multi-point interactions through simultaneous modification with substituents (e.g., perfluoroalkyl chains and quaternary ammonium groups enabling electrostatic interactions[115]) that are less susceptible to contaminants and more likely to interact with specific **PFAS**, incorporation of biological recognition elements (e.g., enzymes, antibodies, or aptamers)[116], and improvement of dispersion stability for detection materials using surfactants structurally dissimilar to **PFAS** (e.g., surfactin,[117-120] organometallic nonclassical surfactant,[121] bolaamphiphile surfactants[122]) are required. Because the 'turn-off type' and 'turn-on type' evaluate changes in fluorescence intensity at same wavelength, it is expected that these detection materials will also have difficulty detecting and identifying between different **PFAS** in the presence of multiple **PFAS**. Based on the intensity ratio of different fluorescent wavelengths, the 'ratiometric type' is expected to enable detection and identification of **PFAS** types and concentrations in the coexistence of multiple **PFAS**. Further, on-site application of this research requires a large number of high-resolution portable fluorometers (USD 20,000–30,000) for detecting specific **PFAS**, making widespread use in aqueous environments impractical. Similar to **2.1. Colorimetric detection**, verification research of **2.2. Fluorescence detection** (with **SPE**) for on-site detection is also underway, and **PFOA** or **PFOS** extracted with in methanol were successfully detected using a composite sensor consisting of a **CD** derivative and an indicator molecule (dye). However, even with long-term **SPE**, it is not possible to completely remove contaminants, making it impossible to detect specific **PFAS** at the ppt level. Further, it cannot identify **PFAS** other than **PFOA** (such as Fluorotelomers or Aqueous Film-Forming Foam). Furthermore, methanol, which cannot be disposed of as general waste, must be used during the implementation of **SPE** and the detection of specific **PFAS**. In verification research of **2.2. Fluorescence detection** for on-site detection, since the detection technology relies on changes in fluorescence intensity at the same wavelength, it is anticipated that detecting and identifying the target **PFAS** from aqueous environments where multiple **PFAS** coexist will be difficult.

The electrodes used in **2.3. Electrochemical detection** enabled high-sensitivity detection of **PFOA**, **PFOS**, and other **PFAS** at ppt–ppb levels in buffers containing specific **PFAS** (e.g., PBS, $KHCO_3$) (without **SPE**). This method showed **LOD** for **PFAS** detection that are close to regulatory levels (several ppt level) set around the world. However, some electrodes with **LOD** close to the ppt level are susceptible to interference from contaminants such as Na^+ and Cl^-, which are likely to competitively adsorb onto electrode surfaces through interactions similar to those with **PFAS**; humic acid, a representative dissolved organic compound; as well as SDS and SDBS, which have structures similar to specific **PFAS**; consequently, the quantification capabilities of specific **PFAS** is easily reduced. Therefore, it is necessary to remove contaminants that reduce the quantitative accuracy of specific **PFAS** using **SPE**, and the surface design combining the formation of multi-point interactions through simultaneous modification with substituents (e.g., perfluoroalkyl chains with carbon chain lengths as short as those of **PFAS** with short carbon

chains[76] and quaternary ammonium groups enabling electrostatic interactions[115]) that are less susceptible to contaminants on the electrode and readily interact with **PFAS** (especially **PFAS** with short carbon chains) and the incorporation of **PFAS**-templated nanostructures (especially **PFAS** with medium to long carbon chain lengths that readily form nanosized templates) is required. There are issues such as the need for a supporting electrolyte for all electrochemical measurements and limitations on use in areas where power supply is unstable. Among these, research on forming nanosized templates on the electrode surface has been able to control the detection ability of different types of **PFAS**; therefore, by combining this material with surface modification of substituents that easily interact with **PFAS**, it is expected that detection and identification will be possible based on the type and concentration of **PFAS** in the coexistence of multiple **PFAS**.

The **SERS** substrates containing **Ag NPs** used for **2.4. SERS detection** was able to detect **PFOA**, **PFOS**, and other **PFAS** mainly in water with high sensitivity at the ppt–ppb level based on slight differences in the peak positions of Raman signals. This method showed **LOD** for **PFAS** detection that are close to regulatory levels (several ppt level) set around the world. The few studies evaluating the effect of contaminants on the developed **SERS** substrate did not show effect from contaminants such as ions and dissolved organic matter present in tap water, soil water, lake water, and urine. In many cases, the effect of contaminants on **SERS** substrates remains unvalidated; therefore, **SERS** substrates exhibiting ppt-level **LOD** must be closely monitored to ensure that the quantification capabilities of specific **PFAS** does not decrease in the presence of contaminants. If the **SERS** substrate is affected by contaminants, it will be necessary to remove the contaminants by **SPE**, which will reduce the quantification capabilities of specific **PFAS**, and simultaneous modification of the **SERS** substrate with multiple substituents (e.g., perfluoroalkyl chains[76] and quaternary ammonium groups enabling electrostatic interactions[115]) that are less susceptible to contaminants and more likely to interact with specific **PFAS**, surface modification with compounds that are balance the affinity between different **PFAS** (amphiphilic self-assembled monolayer or polymer brushes containing both cationic and hydrophobic domains[123, 124]), or selective host molecules (e.g., β-**CD** and calixarenes[125, 126]) are required. This method relies on slight differences in peak positions of Raman signals originating from structurally similar types of **PFAS**; consequently, in the presence of multiple **PFAS**, shifts in the peak positions of Raman signals can also occur due to competition, making detection and identification based on **PFAS** type and concentration inherently difficult.

Among the four major detection research covered in this review, all except **2.1. Colorimetric detection** has achieved detection and quantification of specific **PFAS** at the ppt level. However, due to detection mechanisms based on nano-level interactions with specific **PFAS**, detection materials with lower **LOD** (ppt level) within each research were easily affected by contaminants such as ions, surfactants, and dissolved organic matter, which reduces the quantitative accuracy of specific **PFAS**. Moreover, in most experiments, aqueous solutions containing dissolved **PFOA** or **PFOS** alone have been used. To date, there have been few research on (1) selective detection and quantification of **PFOA** or **PFOS** (each as a single substance) from aqueous environments containing contaminants, and (2) selective detection and quantification of the target **PFAS** from mixed solutions containing various **PFAS**. In the major detection research, several have been found to be able to detect different types of **PFAS** (each as a single substance) by utilizing the nano-level interactions between **PFAS** and the surface of detection material (**2.1. Colorimetric detection**: F-F interactions[64], **2.2. Fluorescence detection**: hydrophobic interactions[95], **2.3. Electrochemical detection**: selective adsorption to templates on the material surface[106], **2.4. SERS detection**: differences in Raman signal wavelengths derived from vibration of C-F bond in various **PFAS**[109]). These detection research exhibit some responsiveness to contaminants (**2.4. SERS detection** alone is often untested), though their effect is smaller compared to the responsiveness observed during **PFAS** detection. Therefore, it is highly anticipated that (1) selective detection and quantification of **PFOA** or **PFOS** (each as a single substance) from aqueous environments containing contaminants is feasible without **SPE**. Meanwhile, much of current research capable of detecting multiple types of **PFAS** (each as a single substance) relies on changes in absorbance or fluorescence intensity at same wavelength, or slight changes in electrical or Raman signals. Hence, (2) selective detection and quantification of the target **PFAS** from mixed solutions containing various **PFAS** is considered difficult to achieve due to competitive or cancelling interactions between different types of **PFAS** and the detection material. (Different types of **PFAS** cannot be identified, and the decrease in quantitative accuracy is expected.) To achieve selective detection and quantification of specific **PFAS** in (2), it is necessary to develop materials where the wavelengths of absorption, fluorescence, and Raman signals vary significantly depending on the type of **PFAS**, as well as electrodes where the degree of interaction changes substantially according to the type of **PFAS**. To use future **PFAS** detection research in actual aqueous environments, it is necessary to incorporate the latest findings outlined in this review into material design and achieve detection and quantification of **PFAS** without **SPE** under conditions (water containing the mixture of multiple **PFAS**, inorganic anions, dissolved organic matter, among others) resembling actual aqueous environments, such as those described in (1) and (2).

In perspectives of on-site analysis of actual aqueous environments, given the trend toward stricter regulations on specific **PFAS** in various countries around the world (increase in the number of **PFAS** types subject to regulation and further reduction of permissible concentrations in water[127]), it is important (the necessary requirements) to be able to quickly detect, quantify, and identify multiple **PFAS** in the extensive water bodies using a simple method. However, the major research outlined in this review has the challenge of failing to meet the following requirements for on-site analysis of actual water environments. **2.1. Colorimetric detection**: detecting and quantifying **PFAS** at regulatory ppt levels; establishing

technology that do not use **SPE** and organic solvents. **2.2. Fluorescence detection**: identification and quantification of target **PFAS** from water containing multiple **PFAS** and contaminants; establishment of technology not requiring **SPE** and organic solvents. **2.3. Electrochemical detection**: selective **PFAS** detection and quantification in the presence of contaminants; identification and quantification of target **PFAS** from water containing multiple **PFAS**; securing stable power sources across wide areas; preparation of optimal supporting electrolytes for each water body. **2.4. SERS detection**: detection and quantitative capabilities for various **PFAS** species remain unclear; detection and quantitative capabilities for **PFAS** in the presence of contaminants remain unclear; development of **SERS** substrates required for the highly sensitive detection, quantification, and identification of different types of **PFAS**.

To carry out on-site analysis of actual water environments over extensive water bodies, the developed detection technology must be portable so that it can be easily used in each water body. In fact, label-free optical **PFAS** detection technology is being investigated as an emerging technology for portable specific **PFAS** detection.[128-130] While these portable technologies have the potential to become platforms for specific **PFAS** detection due to their low power consumption, they have challenges such as insufficient **LOD** (hundreds of ppt to a few ppb), unknown effects on contaminants, and the need for high levels of expertise in each portable technology (device setup). Although each detection research is beginning to obtain promising results indicating its potential to detect, quantify, and identify multiple **PFAS**, setting up new equipment tailored to each detection research for portability–a requirement for conducting on-site analysis across extensive water bodies–could become a barrier to adoption. Conversely, inexpensive portable spectrophotometers for water quality analysis, necessary for implementation in extensive water bodies, are actually being used at each site.[131-134] Therefore, among the verification research outlined in this reviewed, if the technology capable of detecting and quantifying ppt-level **PFAS** in **2.1. Colorimetric detection** without using **SPE** and organic solvents can be established and the requirements for on-site analysis of actual water environments can be met, it is expected that combining this technology with the portable spectrophotometers will bring us the closest to quickly realizing on-site detection in aqueous environments across the country, where regulations on specific **PFAS** are being strengthened.

Author contributions

Aki Shibata: data curation, funding acquisition, investigation and writing–original draft & editing. Mitsuaki Nuno: data curation, funding acquisition, investigation and writing–review & editing. Tomoka Ishikawa: data curation and investigation. Hitoshi Kasai: data curation, funding acquisition and writing–review & editing. Kouki Oka: conceptualization, data curation, funding acquisition, investigation, supervision, writing–original draft and review & editing.

Conflicts of interest

View Article Online
DOI: 10.1039/D5NR05521K

The author declares no competing financial interest.

Data availability

No primary research results, software or code have been included and no new data were generated or analyzed as part of this feature article.

Acknowledgements

This work was supported by the New Energy and Industrial Technology Development Organization (NEDO), Japan, under the Leading Research Program (No. JPNP14004) and JSPS Grants-in-Aid for Scientific Research (No. JP23H03827, JPJSBP120258801, JP24K01552, JP25K21722, JP22H00328, JP24KF0174, JP25K00058 and JP25K23579) from MEXT, Japan. In addition, this work was partially supported by the Environment Research and Technology Development Fund (JPMEERF20241RA4, 5RB-2502) of the Environmental Restoration and Conservation Agency provided by Ministry of the Environment of Japan. Kouki Oka also acknowledges the support from the Amano Industry Technology Laboratory, the Ozawa and Yoshikawa Memorial Electronics Research Foundation, the Noguchi Institute (NJ202411), the TEPCO Memorial Foundation, the Fujimori Science and Technology Foundation, the Paloma Environmental Technology Development Foundation, the Intelligent Cosmos Academic Foundation, the Kato Foundation for Promotion of Science (KS-3416), Sugiyama Houkoukai, the Shorai Foundation for Science and Technology, the Yamada Science Foundation, the Kenjiro Takayanagi Foundation, the Kansai Research Foundation for Technology Promotion, the Yashima Environment Technology Foundation, the JACI Prize for Encouraging Young Researchers, the Iketani Science and Technology Foundation, the Foundation for Interaction in Science & Technology. Aki Shibata also acknowledges the support from Yamaguchi Educational and Scholarship Foundation, Mishima Kaiun Memorial Foundation.

References

1. Z. Wang, A. M. Buser, I. T. Cousins, S. Demattio, W. Drost, O. Johansson, K. Ohno, G. Patlewicz, A. M. Richard, G. W. Walker, G. S. White and E. Leinala, *Environ. Sci. Technol.*, 2021, **55**, 15575–15578.
2. I. T. Cousins, J. C. DeWitt, J. Gluge, G. Goldenman, D. Herzke, R. Lohmann, M. Miller, C. A. Ng, M. Scheringer, L. Vierke and Z. Wang, *Environ. Sci. Process. Impacts*, 2020, **22**, 1444–1460.
3. X. Jiang, Y. Luo, S. Mu, B. Meng, W. Wang, G. Yu and S. Deng, *Water Res.*, 2025, **268**, 122749.
4. D. M. Wanninayake, *J. Environ. Manage.*, 2021, **283**, 111977.
5. Z.-W. Ke, S.-J. Wei, P. Shen, Y.-M. Chen and Y.-C. Li, *Appl. Clay Sci.*, 2023, **232**.
6. J. Li, B. Xi, G. Zhu, Y. Yuan, W. Liu, Y. Gong and W. Tan, *Environ. Res.*, 2023, **218**, 114980.

DOI: 10.1039/D5NR05521K

7. R. Akai, H. Kasai and K. Oka, *Nanoscale*, 2025, **17**, 9920–9925.
8. T. Ami, K. Oka, S. Kitajima and N. Tohnai, *Angew. Chem. Int. Ed.*, 2024, **63**, e202407484.
9. T. Ami, K. Oka, K. Tsuchiya and N. Tohnai, *Angew. Chem. Int. Ed.*, 2022, **61**, e202202597.
10. X. Liu, S. Liu, W. Qiu, J. T. Magnuson, Z. Liu, G. Yang, H. Chen, Y. Li, X. Xu and C. Zheng, *Sustain. Horiz.*, 2022, **3**, 100027.
11. A. A. Bayode, S. S. Emmanuel, A. O. Akinyemi, O. T. Ore, S. O. Akpotu, D. T. Koko, D. E. Momodu and E. A. Lopez-Maldonado, *Environ. Res.*, 2024, **261**, 119719.
12. Y. Wang, S. B. Darling and J. Chen, *ACS Appl. Mater. Interfaces*, 2021, **13**, 60789-60814.
13. M. Yadav, F. J. Osonga and O. A. Sadik, *Sci. Total Environ.*, 2024, **912**, 169279.
14. K. A. Barzen-Hanson, S. C. Roberts, S. Choyke, K. Oetjen, A. McAlees, N. Riddell, R. McCrindle, P. L. Ferguson, C. P. Higgins and J. A. Field, *Environ. Sci. Technol.*, 2017, **51**, 2047–2057.
15. A. B. Lindstrom, M. J. Strynar and E. L. Libelo, *Environ. Sci. Technol.*, 2011, **45**, 7954–7961.
16. D. Herzke, E. Olsson and S. Posner, *Chemosphere*, 2012, **88**, 980–987.
17. Q. Li, T. Wang, Z. Zhu, J. Meng, P. Wang, S. Suriyanarayanan, Y. Zhang, Y. Zhou, S. Song, Y. Lu and B. Yvette, *Chemosphere*, 2017, **167**, 344–352.
18. S. K. Nayak, K. Bhardwaj, P. K. Verma and S. Yamijala, *J. Phys. Chem. Lett.*, 2025, **16**, 8046–8055.
19. S. Kurwadkar, J. Dane, S. R. Kanel, M. N. Nadagouda, R. W. Cawdrey, B. Ambade, G. C. Struckhoff and R. Wilkin, *Sci. Total. Environ.*, 2022, **809**, 151003.
20. X. Lei, Q. Lian, X. Zhang, T. K. Karsili, W. Holmes, Y. Chen, M. E. Zappi and D. D. Gang, *Environ. Pollut.*, 2023, **321**, 121138.
21. W. Tang, Y. Meng, B. Yang, D. He, Y. Li, B. Li, Z. Shi and C. Zhao, *J. Environ. Sci.*, 2022, **122**, 14–24.
22. J. Sun, X. Jiang, H. Xiang, X. Wang, X. Luo, J. Fu and J. Fan, *J. Environ. Chem. Eng.*, 2024, **12**, 113210.
23. D. Lu, S. Sha, J. Luo, Z. Huang and X. Zhang Jackie, *J. Hazard. Mater.*, 2020, **386**, 121963.
24. Q. Wang, Y. Shao, K. M. Y. Leung, P. K. S. Lam and Y. Ruan, *Mar. Pollut. Bull.*, 2025, **216**, 117993.
25. Y. Cui, S. Wang, D. Han and H. Yan, *TrAC Trends Anal. Chem.*, 2024, **176**, 117754.
26. P. Wang, G. An, I. Carra, F. Hassard, P. Campo Moreno, H. Sakar, M. Jodkowska, D. Wang, B. Jefferson, W. Chu and P. Jarvis, *Sep. Purif. Technol.*, 2025, **355**, 129562.
27. S. Y. Wee and A. Z. Aris, *npj Clean Water*, 2023, **6**, 57.
28. R. F. Menger, E. Funk, C. S. Henry and T. Borch, *Chem. Eng. J.*, 2021, **417**, 129133.
29. C. S. Skaggs and B. A. Logue, *J. Chromatogr. A*, 2021, **1659**, 462493.
30. G. W. Olsen, D. C. Mair, C. C. Lange, L. M. Harrington, T. R. Church, C. L. Goldberg, R. M. Herron, H. Hanna, J. B. Nobiletti, J. A. Rios, W. K. Reagen and C. A. Ley, *Environ. Res.*, 2017, **157**, 87–95.
31. M. Dadashi Firouzjaei, E. Zolghadr, S. Ahmadalipour, N. Taghvaei, F. Akbari Afkhami, S. Nejati and M. A. Elliott, *Environ. Chem. Lett.*, 2021, **20**, 661–679.
32. A. Adewuyi and Q. Li, *Eco Environ. Health*, 2024, **3**, 355–368.
33. J. L. Domingo and M. Nadal, *Environ. Res.*, 2019, **177**, 108648.
34. S. Y. Wee and A. Z. Aris, *Ecotoxicol. Environ. Saf.*, 2023, **267**, 115663.
35. Y. Deng, Z. Liang, X. Lu, D. Chen, Z. Li and F. Wang, *Chemosphere*, 2021, **283**, 131168.
36. K. Steenland, T. Fletcher, C. R. Stein, S. M. Bartell, L. Darrow, M. J. Lopez-Espinosa, P. Barry Ryan and D. A. Savitz, *Environ. Int.*, 2020, **145**, 106125.
37. V. Barry, A. Winquist and K. Steenland, *Environ. Health Perspect.*, 2013, **121**, 1313–1318.
38. A. R. Tursi, B. Lindeman, A. B. Kristoffersen, H. Hjertholm, E. Bronder, M. Andreassen, T. Husoy, H. Dirven, S. Andorf and U. C. Nygaard, *Environ. Res.*, 2024, **256**, 119221.
39. J. C. DeWitt, M. M. Peden-Adams, J. M. Keller and D. R. Germolec, *Toxicol. Pathol.*, 2012, **40**, 300–311.
40. X. Du, Y. Wu, G. Tao, J. Xu, Z. Du, M. Wu, T. Gu, J. Xiong, S. Xiao, X. Wei, Y. Ruan, P. Xiao, L. Zhang and W. Zheng, *Sci. Total Environ.*, 2024, **953**, 175958.
41. C. Lau, J. R. Thibodeaux, R. G. Hanson, M. G. Narotsky, J. M. Rogers, A. B. Lindstrom and M. J. Strynar, *Toxicol. Sci.*, 2006, **90**, 510–518.
42. A. E. Lindell, A. Griesshammer, L. Michaelis, D. Papagiannidis, H. Ochner, S. Kamrad, R. Guan, S. Blasche, L. N. Ventimiglia, B. Ramachandran, H. Ozgur, A. Zelezniak, N. Beristain-Covarrubias, J. C. Yam-Puc, I. Roux, L. P. Barron, A. K. Richardson, M. G. Martin, V. Benes, N. Morone, J. E. D. Thaventhiran, T. A. M. Bharat, M. M. Savitski, L. Maier and K. R. Patil, *Nat. Microbiol.*, 2025, **10**, 1630–1647.
43. V. Polychronidou and R. Nag, *Sci. Total Environ.*, 2025, **1000**, 180428.
44. H. Fiedler, *Environ. Health*, 2023, **1**, 41–52.
45. Q. Wenhui, Y. Ge, C. Ling, N. Shan, L. Yuzhe, F. Di, D. Zhaomin, T. M. Jason, S. Daniel, M. Y. L. Kenneth, Z. Yi, Z. Zhenzhong, F. Lian, Z. Xianming, Z. Yanxu, F. Wenhong, H. Tao, M. Jianmin, W. Minghong, T. Shu and Z. Chunmiao, *Science*, 20025, **390**, 1305–1309.
46. M. G. Evich, M. J. B. Davis, J. P. McCord, B. Acrey, J. A. Awkerman, D. R. U. Knappe, A. B. Lindstrom, T. F. Speth, C. Tebes-Stevens, M. J. Strynar, Z. Wang, E. J. Weber, W. M. Henderson and J. W. Washington, *Science*, 2022, **375**, eabg9065.
47. H. Mezawa, A. Eguchi, M. Yamamoto, N. Tokuda, M. Shima, S. Nakayama, M. Kamijima, E. Japan and G. Children's Study, *Environ. Int.*, 2025, **204**, 109824.
48. A. Y. Lin, S. C. Panchangam and C. C. Lo, *Environ. Pollut.*, 2009, **157**, 1365–1372.
49. G. R. Johnson, M. L. Brusseau, K. C. Carroll, G. R. Tick and C. M. Duncan, *Sci. Total Environ.*, 2022, **841**, 156602.
50. Q. A. Al-Maqtari, A. A. Mahdi, N. Othman, A. E. Noman, L. M. Alsubhi, W. AlAnsi, S. M. Asharuddin, M. K. Talib, S. Supramanium and A. Al-Gheethi, *Results Eng.*, 2025, **28**, 107169.
51. Z. Dong, G. Ji, F. Wang and F. Wang, *J. Environ. Chem. Eng.*, 2025, **13**, 118145.
52. E. Southerland and L. S. Birnbaum, *Environ. Sci. Technol.*, 2023, **57**, 7103–7105.
53. X. Li, M. Fatowe, D. Cui and N. Quinete, *Sci. Total Environ.*, 2022, **806**, 150393.
54. M. Mann, V. Kartseva, C. Stanley, M. Blumenthal, R. Silliboy and B. Berger, *RSC Sustain.*, 2024, **2**, 3967–3972.
55. C. Gao, D. S. Drage, M. A.-E. Abdallah, F. Quan, K. Zhang, S. Hu, X. Zhao, Y. Zheng, S. Harrad and W. Qiu, *ACS ES&T Water*, 2024, **4**, 4881–4892.

56. X. Jin, Z. Wang, R. Hong, Z. Chen, B. Wu, S. Ding, W. Zhu, Y. Lin and C. Gu, *Water Res.*, 2022, **225**, 119147.
57. E. Gagliano, M. Sgroi, P. P. Falciglia, F. G. A. Vagliasindi and P. Roccaro, *Water Res.*, 2020, **171**, 115381.
58. D. Thompson, N. Zolfigol, Z. Xia and Y. Lei, *Sens. Actuators Rep.*, 2024, **7**, 100189.
59. M. Renaud-Young, J. Guegueniat, S. Chaudhuri, M. S. Stietz, E. C. Hicks and R. M. Mayall, *Ground Water Monit. R.*, 2025, **45**, 34–36.
60. A. U. Rehman, M. Crimi and S. Andreescu, *Trends Environ. Anal. Chem.*, 2023, **37**, e00198.
61. B. Qian, J. L. Rayner, G. B. Davis, A. Trinchi, G. Collis, I. L. Kyratzis and A. Kumar, *Ecotoxicol Environ Saf*, 2024, **284**, 116932.
62. Z. Zheng, H. Yu, W. C. Geng, X. Y. Hu, Y. Y. Wang, Z. Li, Y. Wang and D. S. Guo, *Nat. Commun.*, 2019, **10**, 5762.
63. J. Ma, C. Liu, J. Li, Z. An, B. Zhang, W. Hong, C. Ye, M. Li and L.-H. Guo, *Environ. Sci. Nano*, 2025, **12**, 1581–1591.
64. J. Jung, J. Park, J. K. Choe and Y. Choi, *Water Res. X*, 2024, **24**, 100239.
65. X. Xu, M. Ma, X. Zhou, X. Zhao, D. Feng and L. Zhang, *ACS Appl. Mater. Interfaces*, 2024, **16**, 15959–15969.
66. Y. Yang, H. Sun, T. Han, Q. Hao, H. Shen, Y. Jing, X. Liu, S. Mu and H. Zhang, *Anal. Chem.*, 2025, **97**, 10474–10483.
67. N. Yang, X. Lin, X. Zheng, W. Lai, Y. Lin, Z. Zou, Q. Wang and X. Zheng, *Mikrochim. Acta*, 2025, **192**, 134.
68. Q. Liu, Q. Chen, Y. J. Tong, X. Zou, X. Zheng and Z. Gong, *Anal. Chem.*, 2024, **96**, 4673–4681.
69. C. Hou, F. Chen, D. Cheng, S. Zou, J. Wang, M. Shen and Y. Wang, *Chem. Eng. J.*, 2024, **481**, 148467.
70. Q. An, Y. Tan, X. Du, H. Fu, P. J. J. Alvarez and X. Qu, *Sens. Actuators B Chem.*, 2026, **448**, 138926.
71. Y. Cui, N. Zhao, Y. Chen, S. Wang, H. Yan and D. Han, *Mikrochim. Acta*, 2025, **192**, 356.
72. H. Zhao, W. Xue, L. Wang, L. Zhang and X. Xu, *ChemNanoMat*, 2025, **11**, e202500164.
73. T. Y. Guo, H. W. Li, C. X. Zhang and Y. Wu, *Analyst*, 2023, **148**, 3931–3937.
74. Y. Wang, Y. Chen, Q. Meng, R. Ren, L. Jing, H. Li, L. Zhou, Z. Tian, J. Wang and C. Hou, *Sep. Purif. Technol.*, 2024, **332**, 125824.
75. J. Liu, X. Wang, F. Ma, X. Yang, Y. Liu, X. Zhang, S. Guo, Z. Wang, S. Yang and R. Zhao, *Chem. Eng. J.*, 2022, **435**, 134966.
76. C. M. Taylor, M. C. Breadmore and N. L. Kilah, *Sens. Diagn.*, 2023, **2**, 676–686.
77. C. M. Taylor, T. A. Ellingsen, M. C. Breadmore and N. L. Kilah, *Chem. Commun.*, 2021, **57**, 11649–11652.
78. C. M. Taylor, M. C. Breadmore, N. L. Kilah and C. Wentrup, *Aust. J. Chem.*, 2023, **76**, 709–718.
79. R. F. Menger, J. J. Beck, T. Borch and C. S. Henry, *ACS ES&T Water*, 2022, **2**, 565–572.
80. C. Fang, X. Zhang, Z. Dong, L. Wang, M. Megharaj and R. Naidu, *Chemosphere*, 2018, **191**, 381–388.
81. M. Al Amin, Z. Sobhani, S. Chadalavada, R. Naidu and C. Fang, *Environ. Technol. Innov.*, 2020, **18**, 100778.
82. L. Jiang, Z. Huang, J. Xu, L. Zhang and Z. Du, *Chem. Eng. J.*, 2024, **484**, 149355.
83. L. Chun-Ze, A. F. Melissa, C. C. Rosenildo, A. G. John, S. Andreas and B. Philippe, *Anal. Chem.*, 2010, **82**.
84. R. Dalapati, S. Manickam, J. Shi, M. Hunter and L. Zang, *Anal. Chim. Acta.*, 2025, **1341**, 343670.
85. C. Zhao, S. Hussain, J. Li, C. Liu, M. A. Afroz, C. Zhu, Z. Yue, J. Zhang, Y. Hao and R. Gao, *Anal. Chem.*, 2025, **97**, 10027–10037.
86. R. Dalapati, M. Hunter, M. Sk, X. Yang and L. Zang, *ACS Appl. Mater. Interfaces*, 2024, **16**, 32344–32356.
87. R. Dalapati, J. Shi, M. Hunter and L. Zang, *J. Mater. Chem. C*, 2025, **13**, 16753–16762.
88. M. H. Hassan, R. Khan, D. Andreescu, S. Shrestha, M. Cotlet and S. Andreescu, *Adv. Funct. Mater.*, 2024, **34**, 2403364.
89. E. Xu, C. Long, Y. Qiao, Z. Chen, X. Yang and P. Ren, *Inorg. Chem.*, 2025, **64**, 19697–19704.
90. S. Mohammadi, C. Sandoval-Pauker, Z. N. Dorado, T. P. Senftle, R. Pankow and H. Sharifan, *Anal. Chem.*, 2025, **97**, 10075–10084.
91. S. Mohammadi, Z. N. Dorado and H. Sharifan, *ACS Appl. Nano Mater.*, 2024, **7**, 21410–21419.
92. A. Concellon, J. Castro-Esteban and T. M. Swager, *J. Am. Chem. Soc.*, 2023, **145**, 11420–11430.
93. Y. Yang, X. Liu, B. Mu, S. Meng, S. Mao, W. Tao and Z. Li, *Biosens. Bioelectron.*, 2024, **257**, 116330.
94. J. Wang, X. Wan, W. Li, C. Song, Q. Gao, Q. Pan and Y. He, *Mikrochim. Acta*, 2025, **192**, 563.
95. X. Chen, S. Hussain, Y. Tang, X. Chen, S. Zhang, Y. Wang, P. Zhang, R. Gao, S. Wang and Y. Hao, *Sci. Total Environ.*, 2023, **860**, 160467.
96. R. Mayall, M. Stietz, M. Renaud-Young, J. Guegueniat, A. Woods and C. Chen, CA Patent, WO 2025/123135 A1, 2025.
97. R. M. Mayall, M. Renaud-Young, C. Chen, M. Mcdonald, S. Sanchez Garcia and E. C. Hicks, CA Patent, WO 2024/216380 A1, 2024.
98. M. M. Shanbhag, N. P. Shetti, A. Daouli, M. N. Nadagouda, M. Badawi and T. M. Aminabhavi, *Langmuir*, 2024, **40**, 3831–3847.
99. F. Simonetti, R. Buccini, V. Migliorati, M. Mancini, D. Caterino, V. Gioia, M. Agostini, F. Mazzei, A. Ciccola, G. Favero and R. Zumpano, *Environ. Res.*, 2025, **285**, 122208.
100. J. J. Calvillo Solís, S. Yin, M. Galicia, M. S. Ersan, P. Westerhoff and D. Villagrán, *Chem. Eng. J.*, 2024, **491**, 151821.
101. I. R. Comnea-Stancu and J. Frederick van Staden, *J. Environ. Chem. Eng.*, 2024, **12**, 113850.
102. R. Khan, Z. O. Uygun, D. Andreescu and S. Andreescu, *ACS Sens.*, 2024, **9**, 3403–3412.
103. X. Zheng, C. Li, N. Yang, L. Niu, F. Gao and Q. Wang, *Anal. Chem.*, 2025, **97**, 6347–6358.
104. Y. Xu, Q. Yin, N. Du, Y. Yi and G. Zhu, *Mikrochim. Acta*, 2024, **191**, 693.
105. Y. Gao, W. Gou, W. Zeng, W. Chen, J. Jiang and J. Lu, *Microchem. J.*, 2023, **187**, 108378.
106. N. Amin, J. Chen, Q. He, J. S. Schwartz and J. J. Wu, *Sens. Actuat. B-Chem.*, 2024, **420**, 136464.
107. M. Pierpaoli, M. Szopinska, A. Olejnik, J. Ryl, S. Fudala-Ksiazek, A. Luczkiewicz and R. Bogdanowicz, *J. Hazard. Mater.*, 2023, **458**, 131873.
108. D. Lu, D. Z. Zhu, H. Gan, Z. Yao, J. Luo, S. Yu and P. Kurup, *Sens. Actuators B Chem.*, 2022, **352**, 131055.
109. Y. Feng, J. Dai, C. Wang, H. Zhou, J. Li, G. Ni, M. Zhang and Y. Huang, *ACS Appl. Nano Mater.*, 2023, **6**, 13974–13983.
110. J. Kumar, A. Jinachandran, V. K. Ponnusamy, G. G. Huang, A. K. Suresh, H. Noothalapati and R. Panneerselvam, *Appl. Surf. Sci.*, 2024, **674**, 160961.
111. H. Park, J. Park, W. Kim, W. Kim and J. Park, *J. Hazard.*

View Article Online
DOI: 10.1039/D5NR05521K

Mater., 2023, **453**, 131384.
112. J. C. Rothstein, J. Cui, Y. Yang, X. Chen and Y. Zhao, *Sens. Diagn.*, 2024, **3**, 1272–1284.
113. C. McDonnell, F. M. Albarghouthi, R. Selhorst, N. Kelley-Loughnane, A. D. Franklin and R. Rao, *ACS Omega*, 2023, **8**, 1597–1605.
114. C. Li, X. Fang, H. Li and X. Zhang, *ACS Appl. Opt. Mater.*, 2024, **2**, 610–616.
115. P. Ramos, S. Singh Kalra, N. W. Johnson, C. M. Khor, A. Borthakur, B. Cranmer, G. Dooley, S. K. Mohanty, D. Jassby, J. Blotevogel and S. Mahendra, *Environ. Pollut.*, 2022, **294**, 118603.
116. C. Esposito, A. M. Cusano, T. M. Caputo, A. Aliberti and A. Cusano, *ACS Mater. Lett.*, 2026, **8**, 716–741.
117. T. Taira, S. Yanagisawa, T. Nagano, T. Tsuji, A. Endo and T. Imura, *Colloids Surf. B Biointerfaces*, 2017, **156**, 382–387.
118. S. Yanagisawa, T. Imura and T. Taira, *ACS Sustainable Chem. Eng.*, 2023, **11**, 5115–5121.
119. T. Taira, R. Moriyama, K. Sakai, H. Sakai and T. Imura, *Colloids Surf. A Physicochem. Eng. Asp.*, 2024, **702**.
120. W. Q. Qin, Y. F. Liu, H. Z. Gang, J. F. Liu, L. Zhou, S. Z. Yang and B. Z. Mu, *Adv. Colloid Interface Sci.*, 2025, **343**, 103581.
121. S. Bitter, M. Kunkel, L. Burkart, A. Mang, R. F. Winter and S. Polarz, *ACS Omega*, 2018, **3**, 8854–8864.
122. S. Stéphanie, R. Kamil, P. Nelly, M. Jean-Daniel, L. V. Nancy, G. Fabienne and M. Christophe, *Chem. Mater.*, 2008, **20**, 1221–1223.
123. N. Faucheux, R. Schweiss, K. Lutzow, C. Werner and T. Groth, *Biomaterials*, 2004, **25**, 2721–2730.
124. F. Frederix, K. Bonroy, W. Laureyn, G. Reekmans, A. Campitelli, W. Dehaen and G. Maes, *Langmuir*, 2003, **19**, 4351–4357.
125. N. M. Y. Zhang, M. Qi, Z. Wang, Z. Wang, M. Chen, K. Li, P. Shum and L. Wei, *Sens. Actuators B Chem.*, 2019, **286**, 429–436.
126. T. S. Vo, T. T. B. C. Vo and K. Kim, *Micro Nano Syst. Lett.*, 2026, **14**, 1–28.
127. K. K. Arun, H. S. Al Yasi, O. Z. Wada, F. AlMomani and K. A. Mahmoud, *Environ. Sci.: Water Res. Technol.*, 2026, **12**, 121–145.
128. N. Cennamo, L. Zeni, P. Tortora, M. E. Regonesi, A. Giusti, M. Staiano, S. D'Auria and A. Varriale, *Talanta*, 2018, **178**, 955–961.
129. F. Faiz, G. Baxter, S. Collins, F. Sidiroglou and M. Cran, *Sens. Actuators B Chem.*, 2020, **312**, 128006.
130. A. V. Saetchnikov, E. A. Tcherniavskaia, V. A. Saetchnikov and A. Ostendorf, *Photonics Res.*, 2023, **11**, A88–A96.
131. S. Sumriddetchkajorn, K. Chaitavon and Y. Intaravanne, *Sens. Actuators B Chem.*, 2014, **191**, 561–566.
132. B. T. Wittbrodt, D. A. Squires, J. Walbeck, E. Campbell, W. H. Campbell and J. M. Pearce, *PLoS One*, 2015, **10**, e0134989.
133. X. Zhu, L. Chen, J. Pumpanen, M. Keinanen, H. Laudon, A. Ojala, M. Palviainen, M. Kiirikki, K. Neitola and F. Berninger, *Talanta*, 2021, **224**, 121919.
134. E. Jekel Könnel, S. D. Nonno and R. Ulber, *Microchem. J.*, 2025, **214**, 113946.

Data Availability Statement

Miyagi, 12 March, 2026

View Article Online
DOI: 10.1039/D5NR05521K

Prof. Kouki Oka
Institute of Multidisciplinary Research for Advanced Materials,
Tohoku University
Miyagi 980-8577, Japan
Phone: +81-22-217-5812
Fax: +81-22-217-5614
E-mail: oka@tohoku.ac.jp

No primary research results, software or code have been included and no new data were generated or analyzed as part of this feature article.

Sincerely,
Kouki Oka
Professor